Thermal production of self-interacting dark matter

by

Alessio Pizzini

Thesis

for the degree of

Master of Science

Faculty of Mathematics and Natural Sciences
University of Oslo

August 2018

Abstract

It is usually assumed in standard relic density calculations that Dark Matter (DM) is in thermal equilibrium during chemical decoupling [1]. However, this is not always the case. Following [2], a new and more generalized approach to relic density calculations is implemented here, where the assumptions about the DM phase space during freeze-out have been weakened. Computing the relic density by means of solving a coupled system of differential equations, we discuss the implications of this improved analysis in terms of how the relic density changes and how this affects the parameter space of the particle physics models describing DM in different scenarios.

Relic density calculations have been implemented within the general framework of DarkSUSY, a Fortran package for DM-related calculations. The improved approach to relic density calculations is extensively tested on the so called "scalar singlet" model, after which a particular emphasis is given to Self-Interacting Dark Matter (SIDM) models.

In order to study the phenomenology of such models it has recently been added a module to the DarkSUSY package that allows to numerically compute the main properties of SIDM candidates. The most important aspects implemented here are the DM self-interaction cross section, mediated by a new type of light bosonic particle, as well as the genesis of DM in the early universe. In these models, similar to the case of more standard DM candidates, the DM particles are thermally produced in the early universe. At high temperatures, chemical equilibrium with the heat bath is maintained via annihilation and creation processes. The point at which these processes stop, known as chemical decoupling or freeze-out, then typically sets the relic density of DM as measured today. Due to the presence of the light mediators, however, the annihilation rate is strongly enhanced for small DM velocities by the Sommerfeld effect. For part of the parameter space this implies that there will be a second period of DM annihilations, at much later times, which significantly lowers the DM abundance compared to what is expected from the standard calculation.

I would like to thank my supervisors, Andrzej Jan Hryczuk and Torsten Bringmann for introducing me to the field of Dark Matter.
I am also grateful to all the teaching staff at the Department of Physics at UiO, especially to Morten Hjorth-Jensen and Susanne Viefers, as well as to my fellow Master students for the exchange of ideas we had, especially Giovanni Pederiva, for the countless discussions about physics, computer science, world history and music theory.
I am extremely grateful to my parents Paolo and Mara for their support during these years.
Above all, I am infinitely grateful to Wolfgang Amadeus Mozart for all the joy his music has always brought to me.

Contents

Chapter 1

Introduction

There is firm evidence that DM is about five times as prevalent as ordinary matter. This is inferred in various independent ways, such as rotational velocity curves in galaxies, gravitational lensing, velocity distribution of galaxies within galaxy clusters or, most importantly, the Cosmic Microwave Background (CMB). While most likely a new elementary particle, the nature of DM is still a matter of debate: no direct or indirect detection experiment has yet reported any uncontroversial DM signal beyond the purely gravitational evidence.

The FORTRAN package DarkSUSY has been developed to numerically calculate properties of supersymmetric DM, historically the most popular DM candidate, as well as to make detailed predictions for various experiments. These can then be compared with real particle and astrophysical measurements in order to test the model. A new modular version of DarkSUSY, not limited anymore to supersymmetric theories, has recently been released [3].

Recently, considerable attention has turned to a class of alternative models where DM experiences a significant amount of self-interaction. This is motivated both by direct though controversial observational support (namely unexpected DM density profiles around galaxy cores and DM distributions which are spatially offset from the luminous mass distribution of their galaxy), and more indirectly by the fact that such models would alleviate the most pressing discrepancies between observations and predictions of the cosmological concordance model [4].

The standard reference for relic density calculations is the Gondolo-Gelmini paper [1], where DM is assumed to be in local thermal equilibrium with Standard Model (SM) particles in the period when annihilation processes with SM particles take place. Following [2], we implemented a treatment of the Boltzmann equation which generalizes the standard calculations to a situation where the assumption that DM is in thermal equilibrium with SM during freeze-out is not necessarily true. As shown in section (6.1), weakening the assumptions used in the implementation of the Boltzmann equation in this way results in a significantly different relic density in certain regions of the parameter space for different particle physics modules.

This improved approach to relic density calculations has been applied to different particle physics models, with a particular emphasis for a Self-Interacting Dark Matter model where DM particles interact through the exchange of a new type of light bosonic particle. In a similar fashion to most DM candidates [1], these particles are thermally produced in the early Universe, when the annihilation and creation processes $\chi\chi \leftrightarrow \phi\phi$ ceased to be effective, hence setting the DM relic density. However, the presence of the light mediators enhances the annihilation rate at small DM velocities and in certain regions of the parameter space (via Sommerfeld enhancement). For these regions of the parameter space this implies that there will be a new period of DM annihilation, at much later times, which lowers the DM abundance by more than two orders of magnitude compared to what is expected from the standard calculation [5]. This happens after kinetic decoupling, when the DM particles have kinetically decoupled from the mediator (or other standard model particles) and therefore start to cool down even faster as the universe expands.

Chapter 2

What is Dark Matter?

2.1 Motivation and Evidence

If we assume that there is no additional matter component in the Universe other than visible matter then standard cosmology fails to explain several astrophysical measurements on a very large range of scales. Here we list the main discrepancies between predictions and astrophysical measurements, ranging from local mass density fluctuations, i.e. density measurements which are averaged over a few parsecs, which is currently the smallest scale we can probe, to the structure formation of the largest known structures in the Universe.

- **Velocity dispersion in galaxy clusters**:

  This is historically the first hint suggesting the presence of a significant yet not detected contribution to the mass of the Universe [6]. Applying the virial theorem to the velocity distribution of galaxies in a galaxy cluster, the bare luminous mass is not sufficient to explain how is the cluster gravitationally bound. This can be explained by requiring an additional non-luminous mass component present within the galaxies.

- **Gravitational lensing**:

  Large amounts of mass are able to bend the light emitted from sources in the background in a significant way. A statistical analysis on the deformation of the image of galaxies and other sources in the background can provide detailed information about the distribution of mass in the Universe. This has been compared with the distribution of luminous matter, resulting in strong indications for large amounts of non luminous matter [7].

- **Rotational curves**:

  By simply applying the classical (Newtonian) law of gravity to the orbit of stars within rotating galaxies we can infer the distribution of the sources of

gravitational potential and compare it to the luminous mass distribution. In a galaxy where most of the mass is concentrated in the center, the velocity of stars orbiting the center decreases with the square root of the distance from the center, a behavior which takes the name of "Keplerian decline". However, in most cases the observed velocity of stars remains constant out to very large radii [7]. The mass distributions inferred from the rotational curves of most galaxies present a noticeable mismatch with the distribution of luminous matter both in the total amount and in the distribution as a function of the distance from the center of the galaxy. To explain the data, galaxies must have enormous dark halos made of unknown DM, making up about 95 % of the mass of galaxies.

- **Cosmic Microwave Background (CMB)**:

  CMB consists in the residual electromagnetic radiation from an early stage of the Universe. The photons underwent oscillations that froze in just before decoupling from the baryonic matter, which took place roughly 380'000 years after the Big Bang [8].

  The feature of CMB which makes it such a powerful probe of several cosmological data is constituted by its variation in temperature depending on the angular position. These anisotropies are understood to have originated from early perturbations in the gravitational potential, which were dominated by the DM component [9]. Detailed analyses strongly point toward a DM contribution to the total which is about five times larger than the baryonic one [10].

- **Structure formation**:

  In order to study the evolution of the Universe from a uniform and featureless stage in early times to the richness in structures present at current stage intense computer simulations of large structures structure have been used. Such simulations have proven to be very accurate when a DM component was included, provided it was made of non-relativistic particles.

  DM plays a crucial role in structure formation because it only feels gravitational interaction, without any other force opposing it, such as radiation pressure. As a result, DM begins to collapse into a complex network of DM halos well before ordinary matter, which is impeded by pressure forces. Without DM, the formation of galactic structures would not have taken place yet at the current age of the Universe [11].

Let's now consider Einstein's field equations, which describe how the presence of matter and energy influences the structure of space-time:

$$R_{\mu\nu} - \frac{1}{2}Rg_{\mu\nu} + \Lambda g_{\mu\nu} = -8\frac{\pi G}{c^4}T_{\mu\nu}, \tag{2.1}$$

where $R_{\mu\nu}$ is the Ricci curvature tensor, R the scalar curvature, $g_{\mu\nu}$ the metric tensor, Λ the cosmological constant, G Newton's gravitational constant, c the speed of light in vacuum and $T_{\mu\nu}$ the stress-energy tensor.

All the attempts to explain the previously mentioned discrepancies can be divided into two groups: trying to modify the left-hand side of the equation, i.e. modified gravity theories or adding a new, non visible source of curvature in the stress-energy tensor in the right-hand term, i.e. DM.

Although some alternative theories of gravity have managed to explain a few of the observations previously listed, none of them has yet proven to successfully take in account the large variety of local and global effects mentioned above. Conversely, the simple assumption of a new, massive constituent which interacts only weakly with SM can explain all of these observations.

2.2 A Brief History of Dark Matter

As a recent article has pointed out [6], the first attempt of a dynamical estimate of the non-luminous gravitational contribution to the total mass of a galaxy - namely, the Milky Way - has been done by Lord Kelvin in the late 19th century, who treated the stars in our galaxy as a gas of particles and inferred the presence of a missing mass contribution from their velocity dispersion. Elaborating on this research, Poincaré first explicitly mentioned DM (although the original French "matiére obscure" would have been better translated as "murky matter") in 1906 [6].

However, the Swiss-American astronomer Fritz Zwicky is arguably the most famous and widely cited pioneer in the field of DM. By means of Doppler shifts he was able to infer the dispersion of the velocity distribution of galaxies in galaxy cluster; he then used the virial theorem to determine the mass of galaxy clusters already in 1933. Most notable were the results relative to the Coma cluster, for which the estimated mass would have to be about 400 times bigger than the value derived from luminous matter. Zwicky himself proposed a "Dark Matter" component as an explanation [12, 13].

Another important evidence in support of DM was discovered by Vera Rubin and Kent Ford [14] who were able to measure and analyze the rotational curve of the Andromeda Galaxy to an unprecedented precision, showing that a significant amount of non-luminous matter was required to explain such rotational curves.

As for the former, of particular interest is the Bullet Cluster, consisting of two clusters which have collided, described by a group of astronomers in 2006 [15]. Here, the mass distribution inferred from gravitational lensing does not trace the plasma distribution, which is the dominant contribution to baryonic matter, as inferred from X-ray data. Instead, it approximately traces the distribution of galaxies. This has been interpreted as a detection of the two corresponding DM clusters of halos which, due to the lesser degree of self-interaction compared to

plasma, simply passed through each other, while the distribution of plasma was slowed and distorted by a drag force, similar to air resistance.

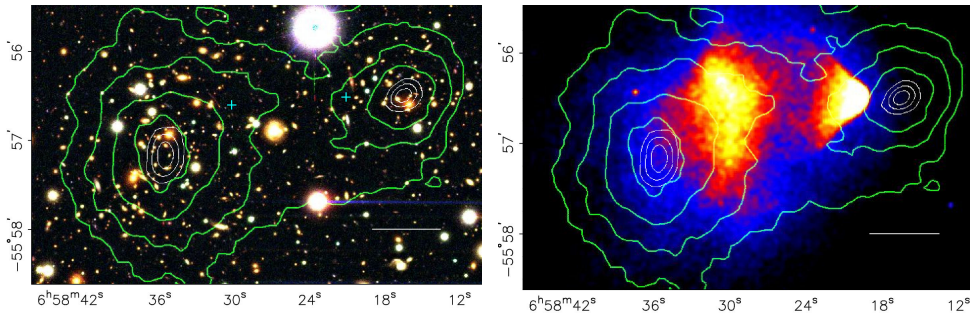

Figure 2.1: The contour plot is relative to the mass distribution as inferred from gravitational lensing, while the background is the distribution of luminous mass as inferred from visible radiation (left) and X-rays (right) [16]

More recent studies have brought in other independent measurements, such as gravitational lensing due to galaxy clusters and the CMB [17, 18].

2.3 Dark Matter Candidates

In order to satisfy the constraints coming from astronomical observations and comparison with numerical simulations, a valid DM candidate must fulfill three main conditions: it must have a close-to-zero coupling to photons and gluons, it must be non-relativistic and stable (relatively to cosmological scales).

Neutrinos were initially the main candidates for DM as they are the only particles within the Standard Model to be stable and not interacting via electromagnetism or strong interaction.

However, in the 1980's numerical simulations of the evolution of large structures of different DM candidates in the expanding Universe entered the picture, bringing in new light. It soon became clear that the primary characteristic of the DM in determining its behaviour in structure formation simulations is whether it is relativistic (Hot DM) or not (Cold DM, often abbreviated in CDM). Any hot DM candidate, including neutrinos, was ruled out as main contributions to DM due to unrealistic results in structure formation simulations.

As early as the 1970's physicists began to look for candidates beyond the Standard Model, namely within the framework of Supersymmetry, which predicts the existence of many new particles, including electrically neutral and/or non-strongly interacting ones. If stable and sufficiently abundant, such particles could entail a strong candidate for DM. The condition on stability can be ensured by selecting the lightest supersymmetric particle, as there are no lighter supersymmetric particles it can decay into. However, constraints from LHC data

have strongly restricted the mass range for supersymmetric particles (at least according to the minimal supersymmetric standard model MSSM), so a broad variety of other candidates for DM have been taken in account more recently.

Some of the other candidates are:

- **Primordial Black Holes**:

  A non-particle candidate for DM consists in Primordial Black Holes (PBH) formed in the early Universe, which are too small to be detected with gravitational lensing [19, 20]. However, most of the theoretically possible mass range for PBH dark matter has been ruled out by various observations [21].

- **Axions**:

  The pseudo-Goldstone bosons relative to a broken global symmetry introduced to tackle the strong-CP problem in QCD provides a valid candidate, being expected to be light and feebly interacting, and have become one of the most popular candidates for DM [22].

- **Kaluza-Klein excitations from universal extra dimensions**:

  As the only specific DM candidate to emerge from theories with extra dimensions [23], the lightest Kaluza-Klein state is a viable candidate for DM, with promising indications about the predicted relic density [24].

- **Sterile neutrinos**:

  While Standard Model neutrinos have been ruled out by numeric simulations (at least as the main constituent of particle DM), this argument does not hold for sterile neutrinos, i.e. neutrinos with right-handed chirality. These hypothetical particles could be produced with a wide range of temperatures depending on their mass (warm DM with $m_\chi \sim keV$ and cold DM with $m_\chi \gg keV$)[6, 25].

Even if the question of the nature of DM remains unsolved, several considerations can be done regardless of its particle physics description. For example, a broad range of electroweak-scale DM candidates, including any stable particle with masses in the MeV-TeV range and interactions mediated by the exchange of electroweak-scale particles, would have a relic abundance (i.e. the amount of mass of a certain species present in the Universe at the current stage, see (4) for a more detailed discussion of the topic) that is roughly equal to the measured density of DM (the so called "WIMP miracle") [26]. This observation has elevated weakly interacting massive particles (WIMPs) to the leading class of candidates for DM [1].

[1] Although the term WIMP was originally intended to include all particle DM candidates, including axions, gravitinos, etc., the definition of this term has since evolved to more often denote only those particles that interact through weak scale force [6].

Chapter 3

Cosmology background

3.1 Friedmann-Robertson-Walker Cosmology

The current understanding of the evolution of the Universe is based on the Friedmann-Robertson-Walker (FRW) cosmological model, which has proven to be so successful to become known as standard cosmology. Its validity is supported by several independent tests, the earliest of which, primordial nucleosynthesis, took place about 10^{-2} sec after the Big Bang [27]. In this section the FRW metric will be derived from general principles.

The observable Universe appears to be homogeneous and isotropic on large scales. This claim has been supported by several observations, including the isotropy of the X-ray background radiation [28], and the distribution of faint radio sources [29]. However, the clearest indication consists in the measurements of the CMB, whose deviations from regularity are of the order of 10^{-5} relatively to the averaged value [10]. Tautologically, there cannot be any available information regarding the homogeneity of regions of the Universe lying outside the observable region. An eventual inhomogeneity of these regions might affect in the future our observable Universe but due to causality we can at least assume that the observable region will remain homogeneous and isotropic for a time comparable to that needed by light to cross it, i.e. of the order of 10^9 yrs [27].

Homogeneity and isotropy do not imply that the Universe is stationary too; in fact, the space-time structure of the Universe does evolve in time. A general metric for a homogeneous, isotropic and time-dependent spacetime is the Friedmann−Lemaître−Robertson−Walker metric:

$$ds^2 = -dt^2 + a^2(t)\left[\frac{dr^2}{1-kr^2} + r^2 d\Omega^2\right], \tag{3.1}$$

with $a(t)$ being the scale factor, r the radial coordinate, Ω the solid angle. The time coordinate t is the proper time measured by an observer at rest in the comoving frame, i.e. the inertial frame in which the observer is instantaneously at

rest. In dimensionless comoving coordinates the parameter k can be set to either -1, 0, +1, respectively describing negative, zero or positive spatial curvature.

It has been established by astronomical observations [30] that the observable Universe is consistent with a flat metric (k=0), so we recover a modified version of the usual flat space of special relativity which is expanding according to the scale factor $a(t)$.

3.1.1 The Friedmann Equations

The next conceptual step is to derive the evolution of the scale factor $a(t)$ by adding an explicit form of the stress-energy tensor to Einstein's equations [1].

Due to the requirements of isotropy and homogeneity the standard approach is to model the energy and matter content of the universe as a perfect fluid, i.e. a medium which is locally isotropic in comoving coordinates. Such a fluid is characterized by the energy-momentum tensor

$$T_{\mu\nu} = \begin{pmatrix} \rho & 0 & 0 & 0 \\ 0 & & & \\ 0 & & g_{ij}p & \\ 0 & & & \end{pmatrix}, \tag{3.2}$$

where p is the pressure.

Or, with one raised index,

$$T^{\mu}_{\nu} = diag(-\rho, p, p, p). \tag{3.3}$$

Before moving on to Einstein's equations it is worth to consider the zeroth component of the energy-momentum conservation condition:

$$0 = \nabla_{\mu} T^{\mu}_{0} = -\partial_0 \rho - 3\frac{\dot{a}}{a}(\rho + p). \tag{3.4}$$

Assuming a generic equation of state of the form $p = w\rho$ with w being some constant, eq.(3.4) becomes

$$\frac{\dot{\rho}}{\rho} = -3(1+w)\frac{\dot{a}}{a}, \tag{3.5}$$

which can be integrated into

$$\rho \propto a^{-3(1+w)}. \tag{3.6}$$

We now consider some physically relevant cases:

- **Matter**:

  It consists of any kind of non-relativistic particles. We can describe matter as a component characterized by zero pressure: $p_M = 0$ and $\rho_M \propto a^{-3}$.

[1] The calculations presented here follow closely follow [31].

The dependency of the number density on the scale factor a can be easily understood as it simply results from the dilution due to the expansion of the Universe.

- **Radiation**:

  In its broadest definition radiation consists in all particles moving at relativistic velocity, as photons do. The equation of state is $p_R = \frac{1}{3}\rho_R$, implying $\rho_R \propto a^{-4}$. We notice that its energy density decreases more quickly compared to matter. This is because on top of the usual decrease in number density due to dilution the energy density is also decreased by the energy loss due to redshift every photon experiences.

- **Cosmological constant**:

  It is defined by the equation of state $p_\Lambda = -\rho_\Lambda$, resulting in a constant energy density. As the other two components have an energy density which is decreasing with time, the vacuum energy must prevail at some point. The Universe is currently that stage.

Taking the trace of Einstein's equations we find the relation $R = -8\pi GT$. Using this relation we can rewrite Einstein's equations as

$$R_{\mu\nu} = 8\pi G\left(T_{\mu\nu} - \frac{1}{2}g_{\mu\nu}T\right). \tag{3.7}$$

Once we insert the energy-momentum tensor we see that due to isotropy only two out of sixteen equations are actually independent, namely the one corresponding to $\mu\nu = 00$ and the one resulting from $\mu\nu = ij$. After a little cleaning up they become:

$$\left(\frac{\dot{a}}{a}\right)^2 = \frac{8\pi G}{3}\rho - \frac{\kappa}{a^2} \tag{3.8}$$

$$\frac{\ddot{a}}{a} = -\frac{4\pi G}{3}(\rho + 3p), \tag{3.9}$$

respectively.

Together these are known as the Friedmann equations.

It is now useful to introduce the Hubble rate as the ratio between the time derivative of the scale factor $\dot{a}$ and a itself at a given time: $H(t) = \frac{\dot{a}(t)}{a(t)}$. Recalling the role of the scale factor a in the FRW metric, we see that the Hubble rate describes how fast the University is expanding.

We can also define the critical density ρ_{crit} as the required value for the total density in order to have a flat Universe:

$$\rho_{crit} = \frac{3H^2}{8\pi G}. \tag{3.10}$$

Rewriting (3.8) in terms of the ratio between the density and the critical density $\Omega = \frac{\rho}{\rho_{crit}}$, which takes the name of density parameter, we have

$$\frac{\kappa}{H^2 a^2} = \Omega - 1. \tag{3.11}$$

It is now straight-forward to see that $\Omega > 1$ implies a positive curvature, while $\Omega < 1$ implies a negative curvature. By definition $\Omega = 1$ implies a flat Universe.

Another interesting way of rewriting (3.8) is the following: we can rewrite the curvature term as a fictitious energy density by defining

$$\rho_C = -\frac{3\kappa}{8\pi G a^2}. \tag{3.12}$$

With this definition, (3.8) takes a very compact way:

$$H^2 = \frac{8\pi G}{3} \sum_i \rho_i. \tag{3.13}$$

This expression can be further simplified by dividing it by H^2 and rewriting all the contributions to energy density as the corresponding density parameters $\Omega_i = \frac{\rho_i}{\rho_{crit}}$

$$1 = \sum_i \Omega_i. \tag{3.14}$$

Now, keeping in mind (3.6), and setting $\kappa = 0$, we see that depending on the value of the scale parameter a the dominant contribution to the Hubble parameter comes from radiation, matter or cosmological constant according to:

$$H^2 \propto \left[\Omega_r + \Omega_m + \Omega_\Lambda\right], \tag{3.15}$$

recalling that $\Omega_r \propto a^{-4}$, $\Omega_m \propto a^{-3}$ and Ω_Λ does not depend on a.

The dynamics of the early Universe were set by radiation, as the density parameter coming from radiation, Ω_r dominated over the others due to the very low value of the scale parameter a. During radiation domination, $a \propto t^{\frac{1}{2}}$ as can be seen by approximating the whole energy density ρ with the dominant radiation component ρ_r and solving (3.8) with this substitution.

At later times, as the value of a decreased, the Universe started to be dominated by the matter contribution, resulting in $a \propto t^{\frac{2}{3}}$. The age of the Universe at which matter and radiation had equal energy density (matter-radiation equality) was about $47'000$ years [32].

At the current stage, the contribution to the total energy density coming from the cosmological constant is the dominant one, even if matter still constitutes a relevant part in the total energy balance. The age of the Universe at which matter and the cosmological constant had equal energy density (often called matter-dark energy equality) was 9.8 ± 1.0 billion years [32].

3.2 Thermodynamics in the Expanding Universe

Proceeding with the analysis of the equilibrium thermodynamics, we consider the number density of a single species, which is defined as:

$$n = \frac{g}{(2\pi)^3} \int f(\mathbf{p}) d^3p, \tag{3.16}$$

where g is the number of internal degrees of freedom and $f(\mathbf{p})$ the phase-space distribution function.

Approximating quantum statistics to the classical Maxwell-Boltzmann distribution we can define:

$$n_{eq} = \frac{g}{2\pi^2} \int \frac{1}{\exp(E(\mathbf{p})) \pm 1} d^3p \approx \frac{g}{2\pi^2} \int \exp(-E(\mathbf{p})) d^3p = \frac{g m^2 T K_2(\frac{m}{T})}{2\pi^2}, \tag{3.17}$$

where K_i stands for the modified Bessel function of the second kind of the i-th order.

Let us now turn our attention to entropy. In the earliest part of the thermal history of the Universe, its constituents were maintained in local thermal equilibrium, hence the entropy per comoving volume was conserved. The expression for the entropy density can be derived as follows[2]: starting from the second principle of thermodynamics we have,

$$TdS = dU + W = d(\rho V) + pdV = d[(\rho + p)V] - Vdp. \tag{3.18}$$

From the condition

$$\frac{\partial^2 S}{\partial T \partial V} = \frac{\partial^2 S}{\partial V \partial T} \Rightarrow dp = \frac{\rho + p}{T} dT, \tag{3.19}$$

it follows that

$$dS = \frac{1}{T} d[(\rho + p)V] - (\rho + p)V \frac{dT}{T^2} = d\left[\frac{(\rho + p)V}{T}\right], \tag{3.20}$$

which defines S up to an additive constant.

Comparing (3.20) with energy conservation

$$0 = d[(\rho + p)V] - Vdp = d[(\rho + p)V] - V\frac{\rho + p}{T} dT = d\left[\frac{(\rho + p)V}{T}\right] = 0, \tag{3.21}$$

we see that in thermal equilibrium the total entropy is conserved.

We can then define the entropy density s as

$$s = \frac{S}{V} = \frac{\rho + p}{T}. \tag{3.22}$$

[2]The calculations presented here follow closely follow [27].

Now, the entropy density is dominated by the contribution of relativistic particles, so we need to compute the right-hand side of the equation in that case.

Given the phase space distribution function $f(\mathbf{p})$ the following expression for the energy density follows automatically

$$\rho = \frac{g}{(2\pi)^3} \int E(\mathbf{p}) f(\mathbf{p}) d^3p, \tag{3.23}$$

where $f(p)$ is the phase space probability density function which, in the relativistic limit ($T \gg m$) becomes

$$\rho = \begin{cases} \frac{\pi^2}{30} g T^4 & \text{for bosons} \\ \frac{7}{8}\frac{\pi^2}{30} g T^4 & \text{for fermions.} \end{cases} \tag{3.24}$$

where g is the number of internal degrees of freedom.

Recalling the state equation for photons or relativistic particles $p = \frac{1}{3}\rho$ and (3.22) we have the final expression for the entropy density

$$s = \frac{2\pi^2}{45} g_{*s} T^3, \tag{3.25}$$

where instead of g we have used the total number of effective massless degrees of freedom g_{*s}, which only takes in account species having $m \ll T$

$$g_{*s} = \sum_{bosons} g_i \left(\frac{T_i}{T}\right)^3 + \frac{7}{8} \sum_{fermions} g_i \left(\frac{T_i}{T}\right)^3, \tag{3.26}$$

and which is a good approximation for this quantity. This is motivated by the fact that the entropy density of a non-relativistic species is exponentially suppressed compared to that of a relativistic one[3].

The values for the degrees of freedom g_{*s} used in the numerical implementation described in the following sections are those by Drees at al. [33]. Here is a comparison of the mentioned results for g_{*s} (marked by "This Result"), with some other results from the literature. Notice the different notation as here h is used instead of g_{*s}.

[3]It can be shown that in the non-relativistic limit the number density can be approximated by $n \approx g\frac{mT}{2\pi}^{3/2} \exp[-m/T]$ [27].

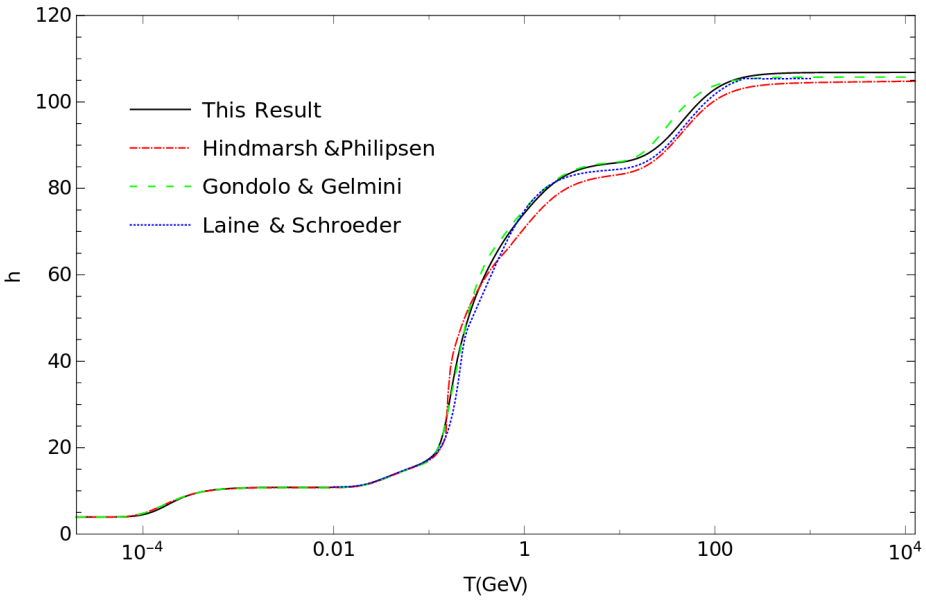

Figure 3.1: Effective numbers of degrees of freedom from [33]

Recalling that in thermal equilibrium the entropy per comoving volume is conserved, i.e. the entropy density scales as the comoving volume $s \propto a^{-3}$, we can define a dimensionless number density Y as $Y = \frac{n}{s}$, which is proportional to the number of some species in a comoving volume when in thermal equilibrium.

The number density of species in thermal equilibrium per comoving volume can be found using eqs. (3.17) and (3.25):

$$Y_{eq} = \frac{n_{eq}}{s} = \frac{45\, g\, m^2 K_2(\frac{m}{T})}{4 g_{*s} T^2 \pi^4}. \tag{3.27}$$

This result is of crucial importance for the thermal history of DM.

Chapter 4

Thermal history of dark matter

4.1 Standard Treatment

According to standard cosmology, the different constituents of the Universe were in thermal equilibrium during most of their thermal history, due to the extremely high density and temperature of the plasma. In the thermal produced DM scenario, the same happened for DM, for which elastic scatterings with standard matter particles as $\chi S \to \chi S$ ensured kinetic equilibrium while annihilation processes $\chi\bar{\chi} \to S\bar{S}$ and $S\bar{S} \to \chi\bar{\chi}$ kept DM particles in chemical equilibrium (we use a notation where χ stands for a DM particle and S for a SM particle). As the Universe expanded and cooled down, such processes became ineffective as interactions with other particles became less frequent, until they were completely negligible. The process of departure from thermal equilibrium takes the name of thermal decoupling and can be separated into kinetic decoupling (i.e. when the velocity distribution of DM particles starts to differ from that of the plasma of standard matter particles) and chemical decoupling (i.e. when the annihilation processes between DM particles and standard matter particles stop to be effective). It is usually assumed that (local) thermal equilibrium was still maintained during chemical freeze-out, however this assumption is not always satisfied, as will be discussed in the following sections.

A simple rule of thumb helping to determine when thermal decoupling took place is that reactions maintaining DM in thermal equilibrium with SM particles are sufficiently effective as long as

$$n\langle\sigma v\rangle \gtrsim H, \tag{4.1}$$

where n is the number density, σ the cross section and v the relative velocity between particles [27]. This can be understood as follows: defining the interaction rate per particle as $\Gamma = n\langle\sigma v\rangle$, we have that the number of interactions

experienced by a species from time t onward is

$$N_{int} = \int_t^\infty \Gamma(t')dt'. \tag{4.2}$$

Having made the common assumption that the Universe is radiation-dominated in this stage (looking up to the Friedmann equation (3.8) we see that in a radiation-dominated Universe we have $a(t) \propto t^{\frac{1}{2}}$) and that the interaction rate scales as $\Gamma \propto T^n$, we have

$$N_{int} = \frac{\frac{\Gamma}{H}\big|_t}{n-2}, \tag{4.3}$$

so for $n > 2$ a particle interacts less than $O(1)$ times at later times than the time when $\Gamma \sim H$ [27]. This thumb rule will be recovered later in this section.

Assumptions

Before embarking on the calculation, it is important to stress a significant source of uncertainty in the following sections: the determination of DM relic density relies on assumptions about the history of the Universe which date back to a period before the Big Bang Nucleosynthesis (BBN), an epoch from which we have no information whatsoever.

The main assumptions in the standard treatment are the following:

- DM particles are thermally produced by interactions with Standard Model particles in the plasma - other production mechanisms have been studied [34] but none of them has reached the popularity of thermal production within the scientific community.

- The entropy of matter and radiation were conserved at the time of the processes considered here - this assumption has been used in the previous chapter to derive an expression for the entropy density (3.25).

- Kinetic equilibrium is maintained during chemical decoupling - this key assumption will prove to be incorrect in some regions of the parameter space [2].

- The decoupling process took place during the radiation-dominated era - this assumption is needed in the derivation of the expression for the entropy density, where the contribution for photons is assumed to be dominant, as well as to motivate the thumb rule (4.1). It will be mentioned in chapter (6.1) that in some cases a second period of annihilation can actually cross over to the matter domination era.

- The SM particles interacting with DM ones are in equilibrium with the thermal bath of photons [35] - it might be that not all SM particles interacted with DM before freeze-out, however, the SM particles which actually interacted with DM are assumed to be in thermal equilibrium with the rest of the thermal bath.
- Only one species of DM particle is taken into account - this is motivated by need for simplification as well as the statistical consideration that if more than one DM constituent contribute to its total amount, it is very unlikely that their relic densities are of similar magnitude, therefore considering only the dominant one is a justified simplification.

For an analytic solution it is indispensable to apply the Boltzmann transport equation, also known as Boltzmann equation, which reads, in its most general formulation[1]:

$$\hat{\mathbf{L}}[f] = \hat{\mathbf{C}}[f], \tag{4.4}$$

where the left hand term is the Liouville operator and the right hand term is the collision operator, which accounts for all interactions between DM and SM particles, including scattering and annihilation processes, as well as eventual DM self interactions.

The general covariant formulation of the Liouville operator is:

$$\hat{\mathbf{L}}[f] = p^\alpha \frac{\partial}{\partial x^\alpha} - \Gamma^\alpha_{\beta\gamma} p^\beta p^\gamma \frac{\partial}{\partial^\alpha}, \tag{4.5}$$

which in the case of an expanding FRW Universe (and hence FRW metric) becomes [36]:

$$E(\partial_t - H_p \cdot \nabla_p) f_\chi, \tag{4.6}$$

so the Boltzmann equation becomes

$$E(\partial_t - H_p \cdot \nabla_p) f_\chi = \hat{\mathbf{C}}[f_\chi], \tag{4.7}$$

where H is the Hubble parameter and E the 0-th component of the four-momentum.

The leading contributions to the collision operator are two-body annihilation processes and elastic scattering, so $\hat{\mathbf{C}}[f_\chi]$ can be split into two contributions and approximated as: $\hat{\mathbf{C}}[f_\chi] \simeq \hat{\mathbf{C}}_{ann}[f_\chi] + \hat{\mathbf{C}}_{el}[f_\chi]$ where these two terms are [2]:

$$\begin{aligned} \hat{\mathbf{C}}_{ann}[f_\chi] = \frac{1}{2g_\chi} \int \frac{d^3\tilde{p}}{(2\pi)^3 2\tilde{E}} \int \frac{d^3k}{(2\pi)^3 2\omega} \int \frac{d^3\tilde{k}}{(2\pi)^3 2\tilde{\omega}} \\ \times (2\pi)^4 \delta^{(4)}(\tilde{p} + p - \tilde{k} - k) \\ \times \left[|\mathcal{M}|^2_{\bar{\chi}\chi \leftarrow \bar{f}f} g(\omega) g(\tilde{\omega}) - |\mathcal{M}|^2_{\bar{\chi}\chi \to \bar{f}f} f_\chi(E) f_\chi(\tilde{E}) \right], \end{aligned} \tag{4.8}$$

[1]The calculations presented here follow [27, 2]. Links to the references will be added for the key statements or when other sources have been used.

and

$$\begin{aligned}\hat{\mathbf{C}}_{el}[f_\chi] = \frac{1}{2g_\chi}\int\frac{d^3\tilde{p}}{(2\pi)^3 2\tilde{E}}\int\frac{d^3k}{(2\pi)^3 2\omega}\int\frac{d^3\tilde{k}}{(2\pi)^3 2\tilde{\omega}} \\ \times(2\pi)^4\delta^{(4)}(\tilde{p}+\tilde{k}-p-k)|\mathcal{M}|^2_{\chi f\leftrightarrow\chi f} \\ \times\left[(1\mp g^{\pm})(\omega)g^{\pm}(\tilde{\omega})f_\chi(\tilde{\mathbf{p}})-(\omega\leftrightarrow\tilde{\omega},\mathbf{p}\leftrightarrow\tilde{\mathbf{p}})\right],\end{aligned} \tag{4.9}$$

where the notation $\omega\leftrightarrow\tilde{\omega},\mathbf{p}\leftrightarrow\tilde{\mathbf{p}}$ means that the same expression is repeated with the substitutions $\omega\leftrightarrow\tilde{\omega}$ and $\mathbf{p}\leftrightarrow\tilde{\mathbf{p}}$.

Having assumed DM to be nonrelativistic, the Bose enhancement/Pauli blocking factors of $1\pm f_\chi$ have been neglected for annihilation processes. Due to momentum conservation, these factors can also be neglected for SM particles.

To further simplify the expressions, we assume CP invariance and kinetic equilibrium. Therefore, $\hat{\mathbf{C}}_{ann}$ can be simplified to [1]

$$\hat{\mathbf{C}}_{ann} = g_\chi E\int\frac{d^3\tilde{p}}{(2\pi)^3}v\sigma_{\bar{\chi}\chi\to\bar{f}f}\left[f_{\chi,eq}(E)f_{\chi,eq}(\tilde{E})-f_\chi(E)f_\chi(\tilde{E})\right], \tag{4.10}$$

where v is the Møller velocity $v_{mol}=(E\tilde{E})^{-1}[(p\cdot\tilde{p})-m_\chi^4]^{1/2}$.

$\hat{\mathbf{C}}_{el}$ has proved to be more difficult to manipulate. However, analytic expressions have been found in the case of highly non-relativistic regimes [37, 38, 2]:

$$\hat{\mathbf{C}}_{el}\simeq\frac{E}{2}\gamma(T)\left[TE\partial_p^2+\left(p+2T\frac{E}{p}+T\frac{p}{E}\right)\partial_p+3\right], \tag{4.11}$$

where the momentum exchange rate $\gamma(T)$ is defined as

$$\gamma(T_{\bar{\gamma}})=\frac{1}{48\pi^3 g_\chi T_{\bar{\gamma}}m_\chi^3}\sum_i\int d\omega k^4(1\mp g_i^{\pm})g_i^{\pm}(\omega)|\mathcal{M}|^2_{t=0}, \tag{4.12}$$

with

$$\left\langle|\mathcal{M}|^2\right\rangle_t=\frac{1}{8k^4}\int_{-4k^2}^0 dt(-t)|\mathcal{M}|^2=16\pi m_\chi^2\sigma_T, \tag{4.13}$$

and with σ_T being the standard transfer cross section $\sigma_T=\int d\Omega(1-\cos\theta)d\sigma/d\Omega$.

However, the term describing elastic scattering processes $\hat{\mathbf{C}}_{el}$ can be for now neglected, as it vanishes in the standard treatment of the Boltzmann equation. The following step is to integrate by parts over momentum space, resulting in:

$$\frac{dn_\chi}{dt}+3Hn_\chi=g_\chi\frac{d^3p}{(2\pi)^3E}\hat{\mathbf{C}}_{ann}[f_\chi]. \tag{4.14}$$

As anticipated, $\hat{\mathbf{C}}_{el}$ disappears from the equation as it does not affect the evolution of the number density.

In order to proceed with the calculations, a crucial assumption is needed: DM is at kinetic equilibrium with SM particles during chemical decoupling, so the following ansatz for the DM distribution can be made:

$$f_\chi = A(\mu) f_{\chi,eq} = \frac{n_\chi}{n_{\chi,eq}}, \tag{4.15}$$

with $A(T)$ a factor depending on the temperature. This ansatz has the following meaning: the phase space distribution of DM f_χ has the same velocity distribution of the plasma of SM particles, but is scaled proportionally to its number density.

Furthermore, the equilibrium distribution is approximated as

$$f_{\chi,eq}(E) \approx \exp(-E/T), \tag{4.16}$$

where the quantum statistics has been approximated to the classical one.

These approximations allow us to rewrite the Boltzmann equation in a more readable form:

$$\frac{dn_\chi}{dx} + 3Hn_\chi = \langle\sigma v\rangle(n_{\chi,eq}^2 - n_\chi^2), \tag{4.17}$$

with the equilibrium number density defined as

$$n_{\chi,eq} = g_\chi m_\chi^2 T K_2\left(\frac{m_\chi}{2T\pi^2}\right), \tag{4.18}$$

and the thermal averaged cross-section as

$$\begin{aligned}\langle\sigma v\rangle = \frac{g_\chi^2}{n_{\chi,eq}^2}\int \frac{d^3p}{(2\pi)^3}\frac{d^3\tilde{p}}{(2\pi)^3}\sigma v_{\bar{\chi}\chi\to\bar{f}f} f_{\chi,eq}(p) f_{\chi,eq}(\bar{p}) = \\ \int_1^\infty d\tilde{s}\sigma_{\bar{\chi}\chi\to\bar{f}f} v_{lab}\frac{2m_\chi\sqrt{\tilde{s}-1}K_1(\frac{2\sqrt{\tilde{s}}m_\chi}{T})}{TK_2^2(\frac{m_\chi}{T})},\end{aligned} \tag{4.19}$$

where K_i are the modified Bessel functions of order i and the Mandelstam variable s is redefined in a dimensionless way as $\tilde{s} = \frac{s}{4m_\chi^2}$.

Here the Maxwell-Boltzmann distribution is baked in the fractional factor while the cross section to be averaged over is σv_{lab}, where the lab velocity v_{lab} is defined as

$$v_{lab} = \frac{\sqrt{s(s-4m_\chi^2)}}{s-2m_\chi^2}, \tag{4.20}$$

and coincides with the previously mentioned Møller velocity $v_{mol} = (E\tilde{E})^{-1}[(p\cdot\tilde{p}) - m_\chi^4]^{1/2}$ in the laboratory reference frame (e.g. where one of the two DM particles is at rest) and in all reference frames obtained via a boost along the

direction of the momentum of the particle moving in the laboratory frame, as shown in appendix Appendix C [2].

The physical meaning of (4.17) is the following: the term proportional to the Hubble rate describes the dilution due to the expansion of the Universe, while the two terms in the brackets take in account the annihilation of DM particles into SM particles and the inverse process.

It is now convenient to introduce the dimensionless quantities

$$x = \frac{m_\chi}{T} \tag{4.22}$$

$$Y = \frac{n_\chi}{s}, \tag{4.23}$$

allowing us to rewrite the Boltzmann equation in a remarkably simple and relatively easily integrable form:

$$\frac{Y'}{Y} = \frac{sY}{x\tilde{H}}\langle\sigma v\rangle\left(\frac{Y_{eq}^2}{Y^2} - 1\right), \tag{4.24}$$

where the entropy density is defined as $s = (\frac{2\pi^2}{45})g_{eff}^S T^3$, $\tilde{H} = \frac{H}{1+g(\tilde{x})}$, with $\tilde{g} = \frac{1}{3}\frac{T}{g_{eff}^S}\frac{dg_{eff}^S}{dT}$ and Y' is primed to denote derivation over x.

As the Universe expanded, the temperature of the plasma fell below m_χ and the DM number density n_χ started to be exponentially suppressed when at equilibrium: $n_\chi \propto e^{m_\chi/T}$ as only the tail of the Maxwell-Boltzmann distribution contributes to n_χ.

To fully understand the physical meaning of eq. (4.17) we can distinguish two different regimes, according to the thumb rule introduced before:

- 1 phase: the Hubble rate H is negligible compared to $\langle\sigma v\rangle n_{eq} \Rightarrow$ eq. (4.17) becomes $\frac{dn_\chi}{dt} = \langle\sigma v\rangle(n_{\chi,eq}^2 - n_\chi^2)$, which simply forces n_χ to follow the equilibrium distribution $n_{\chi,eq}$. In this regime, the leading process in determining the evolution of the DM number density n_χ are the annihilation processes with SM particles. The same happens for the dimensionless number density Y: $Y = Y_{eq}$.

- 2 phase: the Hubble rate H is of the order of $\langle\sigma v\rangle n_{eq}$ or more $\Rightarrow$ the full differential equation ceases to maintain the number density equal to its

[2] It is important to stress that v_{lab} is not the velocity used in the frequently used expansion $\langle\sigma v\rangle = a + \frac{3}{2}\frac{b}{x}$, the latter being instead $v_{CMS} = 2\sqrt{1 - 4\frac{m_\chi^2}{s}}$. In the numerical implementation it is necessary to rewrite v_{lab} as a function of v_{CMS} according to the relation

$$v_{lab} = \frac{v_{CMS}}{2 - 4\frac{m_\chi^2}{s}} \tag{4.21}$$

.

equilibrium value and $n_\chi \neq n_{\chi,eq}$. At this point, the only physical effect in action is the standard dilution of the DM number density n_χ due to the expansion of the Universe and encoded by the term $3Hn_\chi$ in (4.17). However, in the formulation (4.24) the dimensionless number density Y is used instead of the standard number density n_χ. Being defined as the standard number density n divided over the entropy density s, the dimensionless number density Y remains constant when the dilution due to the expansion of the Universe is the only effect reducing the DM number density.

The following picture illustrates what typically happens during freeze-out:

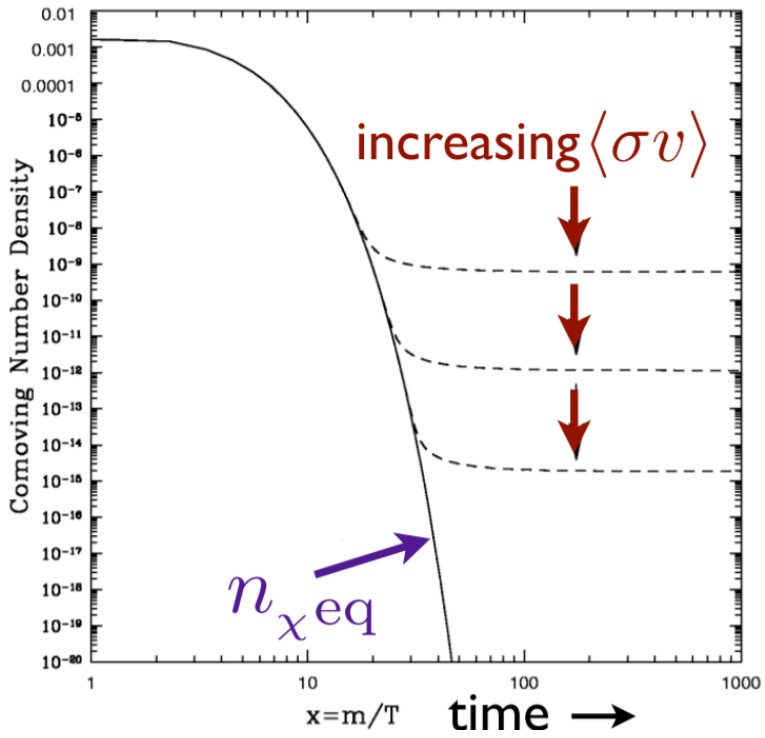

Figure 4.1: The evolution of the dimensionless number density Y as a function of x in the early Universe: the solid line represents the equilibrium distribution, while the dashed line represent the actual evolution of Y for three different values of $\langle\sigma v\rangle$ (from [39])

In the picture above, we see the evolution of the dimensionless number density Y as a function of x. The two regimes described before are clearly visible: Y closely follows the equilibrium density Y_{eq} at first, but then it decouples, assuming a constant value.

We also notice a couple of typical features of chemical decoupling:

- The relic density decreases as $\langle\sigma v\rangle$ increases (more precisely, the relic density is inversely proportional to the annihilation cross section [27]). This

is because a bigger thermal averaged cross section $\langle \sigma v \rangle$ means that the processes keeping DM in chemical equilibrium with SM particles are more effective and will hence continue to be sufficiently strong to maintain DM in chemical equilibrium for a longer time.

- Chemical decoupling of WIMPS typically takes place in a relatively short time around $x_{cd} \simeq 20 - 28$ [40, 5]

These two features will be of central importance in the following chapters as the former is a key concept in the analysis of the outcome of the numerical results presented in (6.1) while the latter does not hold in some regions of the parameter space relative to some particle physics modules.

As kinetic decoupling is usually assumed to have taken place at a much later time than chemical decoupling ($\frac{x_{kd}}{x_{cd}} \simeq 10 - 4000$ [40, 5]), the two processes can be treated separately.

After chemical decouling, DM particled can still be in thermal equilibrium via sufficiently frequent scattering processes. As long as this process is acting, the DM temperature, defined in a non-relativistic regime as [3]

$$T_\chi = \frac{g_\chi}{3n_\chi} \int \frac{d^3p}{(2\pi)^3} \frac{\boldsymbol{p}^2}{E} f(\boldsymbol{p}) \approx \frac{g_\chi}{3m_\chi n_\chi} \int \frac{d^3p}{(2\pi)^3} \boldsymbol{p}^2 f(\boldsymbol{p}), \tag{4.25}$$

is equal to the plasma temperature.

After thermal decoupling, the DM temperature will simply decrease according to the usual scaling for non-relativistic particles: $T_\chi \propto a^{-2}$. Thermal decoupling can be defined as the transition between these two regimes.

However, as this phenomenon is not expected to affect chemical decoupling there's typically no need to include it in the relic density calculations in the standard treatment.

4.2 A Different Approach

4.2.1 Motivation

Despite the success of ΛCDM cosmology, some observations pose a number of problems to the paradigm, namely:

- **"Missing satellites" problem**:

  According to numerical simulations based on standard cosmology, a galaxy of the size of the Milky way (or, more precisely, the DM halo around it) is expected to have a relevant number of dwarf-sized DM satellite subhalos around it. These DM subhalos are central regions of halos that survived

[3] The second, approximated expression is valid in a non-relativistic regime, where $E \approx m$.

strong gravitational tidal forces and dynamical friction during the hierarchical sequence of merging and accretion via which the CDM halos form. However, comparisons with observations revealed that there is a strong discrepancy between abundance of subhalos and luminous satellites of the Milky Way as a function of their circular velocity or bound mass within a fixed aperture: about 50 such subhalos having circular velocity greater than 20 km/s and mass greater than $3 \times 10^8 M_\odot$ within a 570 kpc radius are expected from simulations, compared to the dozen which have been observed around the Milky Way [41]. The difference is even larger if we consider the abundance of satellites in simulated galaxy groups similar to the Local Group [42]. This large discrepancy became known as the "substructure" or the "missing satellites" problem.

- **"Cusp vs core" problem**:

  Concerning the density structure of galaxies, simulations in a collisionless DM scenario predict centrally concentrated cuspy DM halos. However, such predictions contrast with the round, roughly constant density cored halos found in high-quality observations of low surface brightness galaxies and dwarf satellites. In order to reconcile these data with galaxy formation in the context of ΛCDM, processes that alter the shape and density structure of the inner halo are required [43, 44].

- **"Too big to fail" problem**:

  Recently, it was realized that the most massive subhalos in ΛCDM simulations of MW-size halos have an internal density structure that is too concentrated in comparison to the observed brightest MW satellites: the simulated circular velocity profiles increase more steeply and reach their maximum circular velocity at smaller radii than any of the observed ones [45]. No ΛCDM-based model of the satellite population of the Milky Way explains this result [46]. The problem lies in the satellites' densities: it is straightforward to match the observed Milky Way luminosity function, but doing so requires the dwarf spheroidals to have DM halos that are a factor of ~ 5 more massive than is observed.

  On the other hand, those simulated subhalos should be "too big to fail" in forming stars according to our understanding of galaxy formation [4]. Thus, it is extremely surprising why there is no observed analogue to those objects.

Several attempts to tackle these problems have been tried. For example, the "missing satellites" problem can be tackled suppressing the formation of galaxies within existing dwarf halos or suppressing the star formation in dwarf galaxies. Galaxy formation can be held back by increasing the gas entropy before collapse [47, 48, 49]. The "cusp vs core" problem may be addressed by large velocity

anisotropies or reduced central DM densities [50]. The "too big to fail" problem might be solved by either an increased stochasticity of galaxy formation on these scales or a total MW mass 8×10^{11} $M_\odot$ [51, 52].

However, most astrophysical and DM solutions to these problems have shortcomings, or can explain at most two of them, which makes them less attractive on the basis of Occam's razor. A different approach to the problem consists in modifying the CDM paradigm itself by introducing Self Interacting Dark Matter (SIDM) [53].

To solve the "cusp vs core" problem, Spergel & Steinhardt [54] first adopted a SIDM model, in which DM has a large self interaction cross section. It was expected that if DM scatters in the cores of galaxies, then this might result in a flatter central density profile. However, this early attempt fell out of favour due to a mismatch in the shape of the predicted DM halo core compared to observations from gravitational lensing [55] and other incorrect predictions. Recently, it was realized that a new force carrier ϕ (scalar or vector) might naturally mediate a long-range interaction on the scale of the de Broglie wavelength of the WIMPs, leading to a self-interaction cross section for scattering that is much greater than for WIMP annihilation. The studied forces have a variety of scales in them, from the screening scale set by the mass of the carrier particle m_ϕ to the non-perturbative scale set by its coupling α [56]. More specifically, as pointed out by Bringmann, van den Aarssen & Pfommer [4], a simple class of SIDM models may offer a viable solution to all of these problems simultaneously. Such models are characterized by a self-interaction among DM particles described by a Yukawa-like interaction, hence having its characteristic velocity dependence of the transfer cross section [57, 58]. This interaction is mediated by a light messenger.

N-body simulations for a Milky Way-like DM halo have shown that such Yukawa-like interaction result in a small core ($\approx$ 1 kpc) followed by a density profile identical to that of the standard cold dark matter scenario outside of that radius, matching the observed velocity profiles of massive MW satellites [59]. Their key phenomenological properties are velocity-dependent self-interactions mediated by a light vector messenger and different time scales for chemical and kinetical decoupling compared to the standard case [4]. Therefore, the generalized approach to relic density calculations where the assumptions about thermal equilibrium during chemical decoupling have been weakened needs to be applied.

4.2.2 Coupled Boltzmann Equations

Now, in order to obtain a more general formulation of the Boltzmann equation we need to reconsider the assumptions we made in the previous section, namely the ansatz (4.15). Here we assumed that local thermal equilibrium with the thermal bath is maintained during chemical freeze out. If this assumption were not to be valid, another strategy is needed to solve the problem.

The brute force approach would consist in solving the original Boltzmann equation for the full phase space distribution function f_χ. However, as pointed out in [5] only taking in account the second statistical moment of the Boltzmann equation, in addition to the 0-th moment (i.e. the one relative to the number density, already accounted for in the standard treatment) has proven to be sufficiently accurate to to capture the main contribution to the deviation from the standard Gondolo-Gelmini results. The second statistical moment of the DM phase space distribution is defined as:

$$y = \frac{m_\chi}{3s^{2/3}}\left\langle \frac{p^2}{E} \right\rangle = \frac{m_\chi}{3s^{2/3}}\frac{g_\chi}{n_\chi}\int \frac{d^3p}{(2\pi)^3}\frac{p^2}{E}f_\chi(p), \tag{4.26}$$

and is related to the DM temperature T_χ, defined as

$$T_\chi = \frac{g_\chi}{3m_\chi n_\chi}\int \frac{d^3p}{(2\pi)^3}\boldsymbol{p}^2 f(\boldsymbol{p}). \tag{4.27}$$

More precisely, we notice that y is related to the temperature of DM particles according to:

$$T_\chi = y\frac{s^{2/3}}{m_\chi}, \tag{4.28}$$

therefore in the following the term "DM temperature parameter" will often be mentioned when discussing the behaviour of y. It needs to be stressed that y is just proportional to T_χ and even the latter cannot be properly defined as a temperature as the velocity distribution of DM is unknown when not in thermal equilibrium with the thermal bath of SM particles so supposing it to be a Maxwellian distribution is just a well-educated guess.

Integrating (4.7) over $g_\chi d^3p/(2\pi)^3/E$ and $g_\chi^3 p/(2\pi)^3 p^2/E^2$ we finally obtain the two coupled differential equations we were looking for, respectively:

$$\frac{Y'}{Y} = \frac{m_\chi}{x\tilde{H}}\hat{\mathbf{C}}_0 \tag{4.29}$$

$$\frac{y'}{y} = \frac{m_\chi}{x\tilde{H}}\hat{\mathbf{C}}_2 - \frac{Y'}{Y} + \frac{H}{x\tilde{H}}\frac{\langle p^4/E^3\rangle}{3T_\chi}, \tag{4.30}$$

where the two moments of the collision terms are defined as:

$$m_\chi n_\chi \hat{\mathbf{C}}_0 = g_\chi \int \frac{d^3p}{(2\pi)^3 E}\hat{\mathbf{C}}[f_\chi] \tag{4.31}$$

$$m_\chi n_\chi \left\langle \frac{\mathbf{P}^2}{E} \right\rangle \hat{\mathbf{C}}_2 = g_\chi \int \frac{d^3p}{(2\pi)^3 E}\frac{\mathbf{p}^2}{E}\hat{\mathbf{C}}[f_\chi]. \tag{4.32}$$

Now, inserting these analytic expressions we finally obtain the coupled system of equations describing the evolution of the number density of DM and of its temperature parameter y:

$$\frac{Y'}{Y} = \frac{sY}{x\tilde{H}}\left[\frac{Y_{eq}^2}{Y^2}\langle\sigma v\rangle - \langle\sigma v\rangle_{neq}\right] \tag{4.33}$$

$$\begin{aligned}\frac{y'}{y} = &\frac{\gamma(T)}{x\tilde{H}}\left[\frac{y_{eq}}{y} - 1\right] + \frac{sY}{x\tilde{H}}\left[\langle\sigma v\rangle_{neq} - \langle\sigma v\rangle_{2,neq}\right] \\ &+ \frac{sY}{x\tilde{H}}\frac{Y_{eq}^2}{Y^2}\left[\frac{y_{eq}}{y}\langle\sigma v\rangle_2 - \langle\sigma v\rangle\right] + \frac{H}{x\tilde{H}}\frac{\langle p^4/E^3\rangle}{3T_\chi},\end{aligned} \tag{4.34}$$

where $\langle\sigma v\rangle_2$ is defined as:

$$\begin{aligned}\langle\sigma v\rangle_2 = \frac{g_\chi^2}{T n_{\chi,eq}^2}\int \frac{d^3p d^3\tilde{p}}{(2\pi)^6}\frac{p^2}{3E}\sigma v_{\bar{\chi}\chi\to\bar{f}f} f_{\chi,eq}(p) f_{\chi,eq}(\tilde{p}) = \\ \int_1^\infty d\tilde{s}\sigma_{\bar{\chi}\chi\to\bar{f}f} v_{lab}\frac{4\tilde{s}(2\tilde{s}-1)x^3}{3K_2^2(x)} \\ \int_1^\infty d\epsilon_+ e^{-2\sqrt{\tilde{s}}x\epsilon_+}\left[\epsilon_+\sqrt{(\tilde{s}-1)(\epsilon_+^2-1)} + \frac{1}{2\sqrt{\tilde{s}}}\log\left(\frac{\sqrt{\tilde{s}}\epsilon_+ - \sqrt{(\tilde{s}-1)(\epsilon_+^2-1)}}{\sqrt{\tilde{s}}\epsilon_+ + \sqrt{(\tilde{s}-1)(\epsilon_+^2-1)}}\right)\right],\end{aligned} \tag{4.35}$$

and has to be interpreted as the thermal average of a slightly different quantity compared to $\langle\sigma v\rangle$, the difference arising from the different definitions of $\hat{\mathbf{C}}_0$ and $\hat{\mathbf{C}}_2$.

The modified Hubble parameter is defined as

$$\tilde{H} = \frac{H}{\left(1 + \frac{1}{3}\frac{T}{g_{eff}^s}\frac{dg_{eff}^s}{dT}\right)}. \tag{4.36}$$

It is important to stress here that eqs. (4.29) and (4.30) need more information about higher moments of f_χ than the two already accounted for by Y and y. Therefore, eqs. (4.33) and (4.34) contain quantities which have to be somehow determined, namely $\langle\sigma v\rangle_{neq}$, $\langle\sigma v\rangle_{2,neq}$ and $\langle\frac{p^4}{E^3}\rangle$. Following [2], these quantities have been derived from a DM phase-space distribution of the form

$$f_\chi = \frac{n_\chi(T)}{n_{\chi,eq}(T_\chi)}\exp\left(-\frac{E}{T_\chi}\right)\Big|_{T_\chi = y s^{\frac{2}{3}}/m_\chi}, \tag{4.37}$$

obtained assuming that DM particles have a Maxwellian velocity distribution with a different temperature compared to the heath bath (which would be expected in the presence of a significant DM self-scattering [60, 61]).

The resulting ansatzes for the quantities entering eqs. (4.34) and (4.33) are [2]:

$$\langle \sigma v \rangle_{neq} = \langle \sigma v \rangle \big|_{T=ys^{\frac{2}{3}}/m_\chi} \tag{4.38}$$

$$\langle \sigma v \rangle_{2,neq} = \langle \sigma v \rangle_2 \big|_{T=ys^{\frac{2}{3}}/m_\chi} \tag{4.39}$$

$$\left\langle \frac{p^4}{E^3} \right\rangle = \left[\frac{g_\chi}{2\pi^2 n_{\chi,eq}(T)} \int dp \frac{p^6}{E^3} e^{-\frac{E}{T}} \right] \Bigg|_{T=ys^{\frac{2}{3}}/m_\chi} . \tag{4.40}$$

It is important to stress that even though these anzatzes have been derived from the DM phase-space distribution (4.37), they are not strongly dependent on the specific phase-space distribution, as any form of f_χ results in very similar numerical values and hence similar behaviours for $Y(x)$ and $y(x)$ [2].

As a final comment on eqs. (4.33) and (4.34), it is easy to recover the standard Gondolo-Gelmini single equation (4.17) by forcing the condition $y = y_{eq}$ (i.e. kinetic equilibrium with the heat bath), which implies $\langle \sigma v \rangle_{neq} = \langle \sigma v \rangle$. The latter turns eq. (4.33) back to the usual form (4.17) as the presence of $\langle \sigma v \rangle_{neq}$ instead of $\langle \sigma v \rangle$ is the only point where the departure of y from y_{eq} enters the equation describing the evolution of the number density Y.

Chapter 5

Numerical integration

5.1 DarkSUSY

The need for dedicated codes for precise relic density computation is motivated by the high number of processes involved in e.g. cohannihilations (i.e. annihilation processes in the context of a model where a whole family of DM particles χ_i is present). In MSSM, up to 3000 processes can contribute to the relic density when coannihilations are taken into account.

A rather exhaustive list of public DM tools consists in:

- Neutdriver (1995 - not maintained) [62]
- DarkSUSY (2000 - to date) [63]
- micrOMEGAs (2001 - to date) [64]
- IsaRed, IraRes (2002 - to date) [65]
- SuperISORelic (2009 - to date) [66]
- MadDM (2013 - to date) [67]

This analysis will be exclusively carried with DarkSUSY. However, extensive comparisons between different codes have shown that results are generally in good agreement - within a few percent - apart from mass regions close to resonances, where discrepancies are bigger (near the Higgs resonance they can reach 25% [68]).

An advantage DarkSUSY has gained with its latest version (DarkSUSY 6.0) compared to similar numeric tools is that the particle physics module parts of the code has been split from the rest, so the user can simply decide which particle physics module to include at a late stage, i.e. when making the main program

[1]. Therefore, despite its name DarkSUSY allows for a wide variety of particle physics modules to be implemented, and is not limited to supersymmetric models.

Another improvement introduced in DarkSUSY 6.0 is the possibility to use replaceable functions, i.e allowing users to replace any function in DarkSUSY with a user-supplied version.

These features are highlighted in the scheme below, showing the general structure of DarkSUSY.

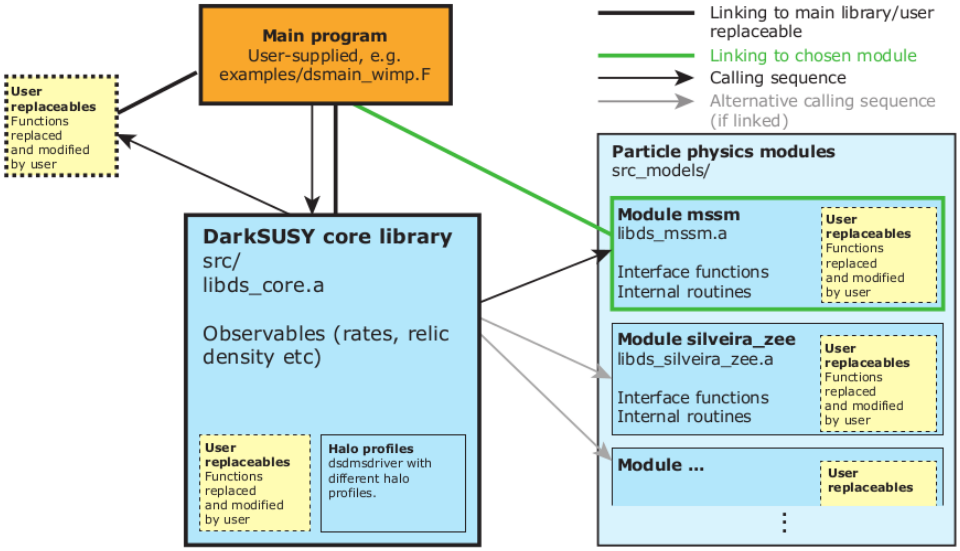

Figure 5.1: The main structure of DarkSUSY is schematized here (from [3])

5.2 Implementation

The goal of this project is to implement the coupled system of equations (4.34) within the framework of DarkSUSY and to validate it against different particle modules.

The implementation has presented a series of additional challenges compared to the already present Boltzmann solver with a single equation, from a much larger number of operations to an increased instability in the evolution of the number density. Eq. (4.17) is already a stiff equation, i.e. numerical solutions are unstable unless the integration step is extremely small. This issue is even more serious in the case of the coupled system of equations.

Here are listed a series of measures taken to tackle these issues:

[1]See the manual [63] for reference.

- A very accurate computation of the two thermal averages $\langle \sigma v \rangle$ and $\langle \sigma v \rangle_2$ ((4.19) and (4.35)) resulted to be the most time consuming part of the code. Therefore, instead of evaluating them every time their value is needed, an interpolation from a table produced before the numerical integration of the equations has been used. As the thermal averages are smooth functions of the parameter x, 1000 tabulated points have proven to be more than sufficient for an accurate interpolation.

- At very early values of x the prefactor $\frac{s}{x\tilde{H}}$, as well as all the similar factors containing the Hubble parameter H at the denominator, are very large, hence enforcing thermal equilibrium (more specifically $Y = Y_{eq}$ and $y = y_{eq}$). However, this can be a problem in a numerical implementation as even a small deviation from the equilibrium value for Y or y, possibly coming from round-off errors can result in a very big derivative due to the large prefactor. While this is still manageable for a single equation, this issue has shown to be even more serious with the coupled system of equations. In order to tackle this problem, the equilibrium condition has been forced to hold by simply setting $Y = Y_{eq}$ and $y = y_{eq}$ for x below a certain threshold, usually between $x = 16$ and $x = 18$, actually solving the coupled system of equations only after that.

- Given that the region of interest, for which the coupled system of equations is actually applied, is highly non-relativistic, the last term, $\frac{H}{x\tilde{H}} \frac{\langle \frac{p^4}{E^3} \rangle_{neq}}{3T_\chi}$, has been neglected in the implementation. As shown in section (6.1), given the good agreement with the literature this assumption has proven to be correct.

- For the scalar singlet model the double integral appearing in the definition of $\langle \sigma v \rangle_2$

$$\langle \sigma v \rangle_2 = \frac{g_\chi^2}{T n_{\chi,eq}^2} \int \frac{d^3p d^3\tilde{p}}{(2\pi)^6} \frac{p^2}{3E} \sigma v_{\bar{\chi}\chi \to \bar{f}f} f_{\chi,eq}(p) f_{\chi,eq}(\tilde{p}) = \int_1^\infty d\tilde{s} \sigma_{\bar{\chi}\chi \to \bar{f}f} v_{lab} \frac{4\tilde{s}(2\tilde{s}-1)x^3}{3K_2^2(x)} \int_1^\infty d\epsilon_+ e^{-2\sqrt{\tilde{s}}x\epsilon_+} \left[\epsilon_+ \sqrt{(\tilde{s}-1)(\epsilon_+^2-1)} + \frac{1}{2\sqrt{\tilde{s}}} \log\left(\frac{\sqrt{\tilde{s}}\epsilon_+ - \sqrt{(\tilde{s}-1)(\epsilon_+^2-1)}}{\sqrt{\tilde{s}}\epsilon_+ + \sqrt{(\tilde{s}-1)(\epsilon_+^2-1)}} \right) \right], \tag{5.1}$$

can be written in a different way by using the analytic solution for part of the integral, following the numerical calculations done in [2]:

$$\langle\sigma v\rangle_2 = \int_1^\infty d\tilde{s}\sigma_{\bar{\chi}\chi\to\bar{f}f}v_{lab}\frac{4\tilde{s}(s\tilde{s}-1)x^3}{3K_2^2}\left(\frac{\sqrt{(\tilde{s}-1)s}K_2^2(x)}{2\tilde{s}x}+\right.$$
$$\left.\int_1^\infty d\epsilon_+ e^{-2\sqrt{\tilde{s}}x\epsilon}\frac{1}{2\sqrt{\tilde{s}}}\log\left(\frac{\sqrt{\tilde{s}}\epsilon_+-\sqrt{(\tilde{s}-1)(\epsilon_+^2-1)}}{\sqrt{\tilde{s}}\epsilon_+-\sqrt{(\tilde{s}-1)(\epsilon_+^2-1)}}\right)\right), \tag{5.2}$$

with the advantage of reducing the number of operations in the most time-consuming part of the calculations.

However, at the very high values of x used in the SIDM model, a numeric issue arises as the integral in ϵ and the partial analytical result become extremely similar in absolute value but opposite in sign, to the point where these two quantities differ only on the sixth digit. Then the value of the whole thermal average becomes extremely sensitive to roundoff errors or approximations in the computation of the integral in ϵ. To prevent this issue the original formulation of $\langle\sigma v\rangle_2$ has been used instead, which is less sensitive to such issues even at high x.

At even higher values of x ($x > 10^9$) the issue with the difference between two large numbers reappears as the two terms $\epsilon_+\sqrt{(\tilde{s}-1)(\epsilon_+^2-1)}$ and $\frac{1}{2\sqrt{\tilde{s}}}\log\left(\frac{\sqrt{\tilde{s}}\epsilon_+-\sqrt{(\tilde{s}-1)(\epsilon_+^2-1)}}{\sqrt{\tilde{s}}\epsilon_++\sqrt{(\tilde{s}-1)(\epsilon_+^2-1)}}\right)$ are extremely close in absolute value but opposite in sign and as the quantity to be integrated is their sum, an extremely precise evaluation of these quantities is needed, which is not supported anymore by the code, so the result of the integral becomes a random number assuming positive or negative values at different evaluations. This problem might have been mitigated by using higher precision number formats but a more radical approach has been preferred to tackle this issue: the expression (5.1) has been expanded in power series in $\tilde{s}$ and ϵ_+ in order to find the leading order deviation in the two similar quantities and therefore the main contribution to the integral. This approach provided excellent precision results, as discussed in Appendix D.

- In order to find the correct thermal averaged cross section for the scalar singlet model, the evolution of the DM number density has been computed several times varying the cross section (or the coupling constant, which then affects the cross section itself). The correct value is found in DarkSUSY via a binary search which stops when the computed relic density is sufficiently close to the result from Planck: $\Omega_\chi h^2 = 0.1193 \pm 0.0014$ [30]. However, while in the standard DarkSUSY code the initial guess for the coupling constant λ relative to the scalar singlet model is fixed, in the numerical implementation used here it has been preferred to start from the value which resulted in the correct relic density in the standard Gondolo-Gelmini

treatment as the initial guess, with the effect of drastically reducing the number of attempts before finding the final value. As the coupled system of equations requires many more operations and is therefore more time-consuming than the standard Gondolo-Gelmini calculations, this procedure has been useful to reduce the total elapsed time. This has been implemented by interpolating a table of values of the coupling constant λ for different DM masses found by the standard DarkSUSY routine.

- In order to solve the coupled differential equations numerically, an ODE solver by Shampine and Gordon [69] has been used. This ODE solver is a FORTRAN90 library which solves a system of ordinary differential equations, with a modified Adams linear multistep method.

The results of the code relative to the "generic WIMP" and "scalar singlet" modules (introduced in (6.1)) have been compared to the standard DarkSUSY results or to results from the literature. More specifically, in the case of the scalar singlet model, the results have been compared with the Mathematica code implementing the coupled system of equations used to produce the plots in [2]. While the agreement in the actual results will be discussed in the next section, it can be already mentioned that thanks to the efficiency of the FORTRAN language and the careful implementation of the coupled equations the elapsed time has been reduced by a factor of $\approx 10^3$.

Chapter 6

Results

In this section three different particle physics modules will be considered, each one of them describing a different candidate for particle DM. Given the modular structure of DarkSUSY 6.0, it is possible to simply link in the modified Boltzmann solver to each physics particle module to analyze the difference.

The first one, the so called generic WIMP module, only serves the purpose to test the proper functioning of the modified version of the Boltzmann solver in a situation where no effect deriving from the improved approach in relic density calculations is expected. Similar analyses can be found in the literature [33].

The second model, which takes the name of scalar singlet, shows the effects of the improved treatment of relic density calculations in an clear way. The results here can be compared with the analysis done in [2].

The third and last particle module, where Self-Interacting DM is analyzed shows how a second period of DM annihilation at late times is only visible thanks to the improved treatment of relic density calculations.

6.1 Validation

6.1.1 Generic Wimp Model

The purpose of this comparison is to check the precision of the new Boltzmann equation solver in a simple particle physics scenario. The standard Boltzmann solver used in DarkSUSY is meant to be substituted with one which allows for the integration of two coupled differential equations in two different quantities, the number density and the second moment of the phase space distribution function of DM. However, in this preliminary test, the standard Gondolo-Gelmini single equation (4.24) is implemented, so no deviations from the results of the standard DarkSUSY code are expected.

Theoretical background

The module generic wimp is the simplest example of a particle physics library that the DarkSUSY core library can link to. Rather than being based on an actual particle physics model, it mostly serves to provide an illustration of how the functionalities of DarkSUSY can be used in phenomenological studies of vanilla WIMP DM, when only providing the absolute minimum of input parameters. [3]

For the purposes of relic density calculations, a generic WIMP model in DarkSUSY is fully defined by the mass m_χ of the DM particle, a flag stating whether the DM particle is its own anti-particle or not and a constant annihilation rate σv, along with the dominant annihilation channel into SM particles.

A simple result which can be obtained by this model is the annihilation rate σv required to obtain a DM relic abundance matching the results from Planck, $\Omega_\chi h^2 = 0.1193 \pm 0.0014$ [30].

Numerical results

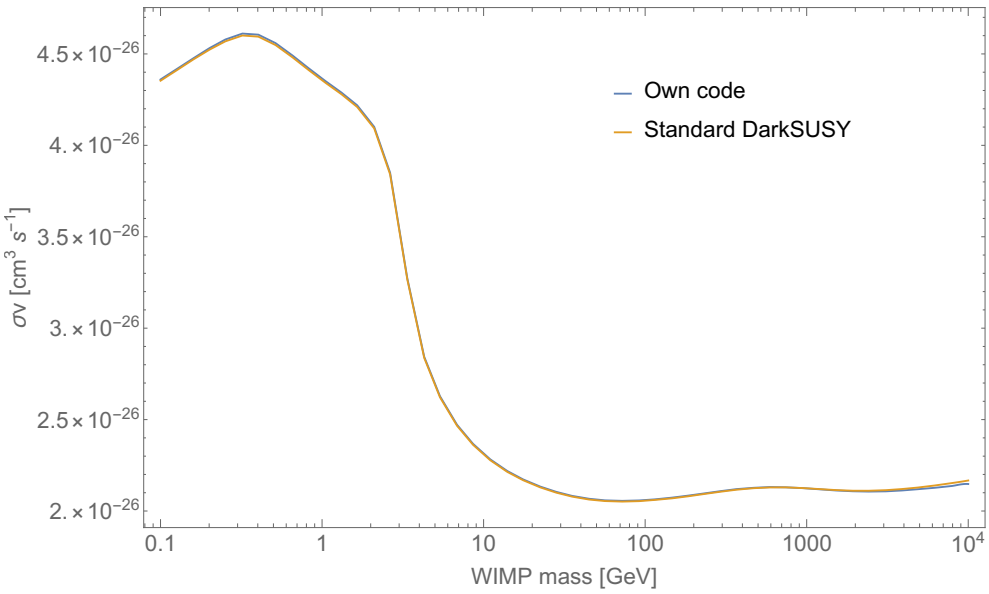

Figure 6.1: Generic WIMP model: the two lines are perfectly overlapping

Being a rather featureless particle physics model, no relevant features are visible in the plot, apart from the effect of the change of the number of degrees of freedom with the temperature, which can be understood as follows. due to the definition $x = \frac{m_\chi}{T}$, at lower values of the WIMP mass m_χ the chemical decoupling, which always takes place at similar values of x, happens at lower values of T. Now, comparing this plot (6.1) with the one showing how the degrees of freedom vary with the temperature (3.1) and keeping in mind the definition of the entropy

density (3.25), where the number of effective degrees of freedom is present at the numerator, we see that the number of effective degrees of freedom and hence the entropy density s and the whole prefactor in front of $\langle\sigma v\rangle$ is smaller at low T, so this needs to be compensated with a larger value of $\langle\sigma v\rangle$ in order to get the correct relic density.

The main point of this comparison, however, is to validate the precision of the part of the code integrating the Boltzmann equation. This has been confirmed by the good agreement with the standard DarkSUSY results.

6.1.2 Scalar Singlet Model

With this physics particle module we can actually test the effect of the improved way of computing the relic density implemented in DarkSUSY comparing results with the analysis carried in [2] where the coupled system of equations (4.33), (4.34) has been implemented in Mathematica.

Theoretical background

A more interesting example of a non-supersymmetric DM candidate which can be tested in DarkSUSY 6.0 is the Silveira-Zee scalar singlet model [70]. This DM candidate (originally named scalar phantom and also known as singlet Higgs DM) is described by a Lagrangian where a gauge-singlet real scalar field S is added to the standard model:

$$\mathcal{L}_{SZ} = \mathcal{L}_{SM} + \frac{1}{2}\partial_\mu S \partial^\mu S - \frac{1}{2}\mu^2 S^2 - \frac{1}{2}\lambda S^2 H^\dagger H, \tag{6.1}$$

where H is the standard Model Higgs doublet.

After electroweak symmetry breaking, the S boson acquires a tree-level mass

$$m_S = \sqrt{\mu^2 + \frac{1}{2}\lambda v_0^2}, \tag{6.2}$$

where $v_0 = (\sqrt{2}G_F)^{-\frac{1}{2}} = 246.2$ GeV.

The annihilation cross section of pairs of DM particles to SM ones (apart from hh final states) is given by [71]

$$\sigma v_{CMS} = \frac{2\lambda_s^2 v_0^2}{\sqrt{s}} |D_h(s)|^2 \Gamma_{h\to SM}(\sqrt{s}), \tag{6.3}$$

where the propagator $\Gamma_{h\to SM}(\sqrt{s})$ is the partial decay width of a SM Higgs boson of mass $\sqrt{s}$

$$|D_h(s)|^2 = \frac{1}{(s - m_h^2)^2 + m_h^2 \Gamma_h^2}, \tag{6.4}$$

where the total width Γ_h above includes the contribution from $h \to SS$ processes for $m_\chi < \frac{m_h}{2}$. On the other hand, $SS \to hh$ processes, which take place at $m_\chi > m_h$, lie outside our kinematic region of interest.

As for the elastic scattering processes, DM scattering with all SM fermions are taken into account. The scattering process is only mediated by a Higgs boson in the t-channel, so its squared amplitude is

$$|\mathcal{M}_{Sf\to Sf}|^2 = \frac{N_f \lambda^2 m_f^2}{2} \frac{4m_f^2 - t}{(t - m_h^2)^2}, \tag{6.5}$$

where the subscript f marks quantities related to the SM fermion, N_f is the color factor, set to 3 for quarks and to 1 for leptons.

Averaging over the transferring momentum according to:

$$\left\langle |\mathcal{M}|^2 \right\rangle_t = \frac{1}{8k^4} \int_{-4k_{cm}^4}^{0} dt(-t)|\mathcal{M}|^2, \tag{6.6}$$

we find

$$\left\langle |\mathcal{M}|^2 \right\rangle_t = \sum_f \frac{N_f \lambda^2 m_f^2}{8k^4} \left[\frac{2k_{cm}^2 - 2m_f^2 + m_h^2}{1 + \frac{m_h^2}{4k_{cm}^2}} - (m_h^2 - 2m_f^2) \log\left(1 + 4\frac{k_{cm}^2}{m_h^2}\right) \right], \tag{6.7}$$

where the center of mass momentum k_{cm} is defined as $k_{cm}^2 = (s - (m_\chi - m_f)^2)(s - (m_\chi + m_f)^2)/(4s)$, with $s = -(p_1^2 + p_2^2)$.

In an analogous fashion to what done with the generic WIMP module, we can study the behavior of the required coupling constant λ to have a correct relic density as a function of the DM mass m_χ.

Doing so, we see a sharp decrease in the required value of λ around $m_\chi \simeq \frac{m_h}{2}$, corresponding to the resonance for the process $\chi\chi \to h$.

The GAMBIT collaboration has recently presented a comprehensive study [72] of the scalar singlet model where experimental constraints from direct, indirect and accelerator searches for DM are taken into account. Interestingly, the region in parameter space which emerged to be the most promising for a DM candidate is characterized by a DM particle m_χ which is about half of the Higgs boson mass and where the process setting the current relic DM density is set by the resonant annihilation of two DM particles through an almost on-shell Higgs boson.

This very region is also of particular importance for relic abundance calculations as here the scattering processes are much less effective than usual, due to the lower coupling constant λ, therefore kinetic decoupling takes place earlier, almost coinciding with chemical decoupling. This region will hence be studied with particular care in the following section.

Numerical results

Analogously to (6.1) it is interesting to plot the required value for the coupling constant λ in order to get the correct relic density as a function of m_χ.

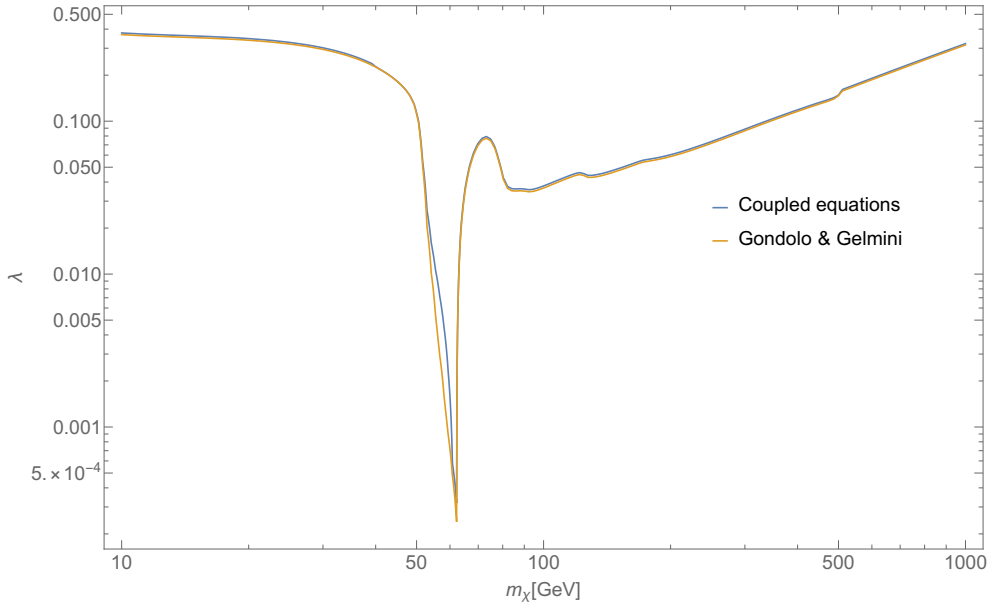

Figure 6.2: Here is a plot of the needed value for the coupling constant λ as a function of the DM mass m_χ (compare with fig. 5 in [3]) according to the standard Gondolo-Gelmini relic density calculations and as computed in the improved treatment.

Compared to fig. (6.1), the behaviour of the coupling constant λ as a function of the WIMP mass m_χ is much richer in features, the most noticeable one being the central dip, corresponding to $m_\chi \simeq \frac{m_h}{2}$. Here the required coupling constant λ is reduced by about two orders of magnitude compared to most of the DM mass range due to a resonance with the annihilation process $\chi\chi \to H$, which strongly enhances DM annihilation processes, hence reducing the required coupling constant λ to obtain the correct relic density.

We also notice a significant discrepancy between the results computed according to the two different approaches only in the region close to the Higgs resonance.

As mentioned before, this is the most interesting region of the parameter space to see the effect of the improved approach of computing relic density calculations, so in the following plot a comparison between the results from the standard Gondolo-Gelmini calculations as implemented in the standard version of DarkSUSY against the results from the improved treatment is shown in the region close to the Higgs resonance.

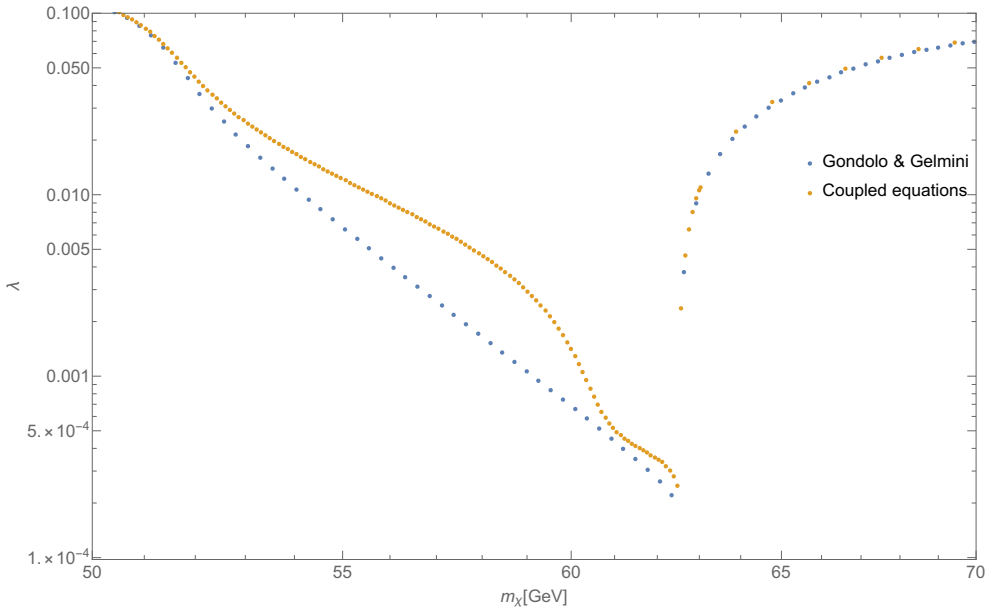

Figure 6.3: Here is a zoom on the region in the mass range for which there is a noticeable departure of the needed value for the coupling constant λ compared to the standard Gondolo-Gelmini relic density calculations. It has been preferred to plot the single points rather than an interpolation as done in the previous plots, due to the discontinuity present here.

As shown in the plot, the difference between the required coupling constant λ in the standard Gondolo-Gelmini calculations and in this improved way of computing the relic density is very noticeable, the ratio between the two quantities reaching a factor of ≈ 2 at $x \simeq 58$.

Qualitative arguments can help to understand why this discrepancy appears close to the Higgs resonance relative to the process $\chi\chi \to H$: here, DM annihilation processes are strongly enhanced, hence a much lower coupling constant λ is needed to obtain the correct relic density. The decrease in the value of λ, however, makes heat exchange via scattering processes less efficient, to the point when kinetic decoupling is not maintained anymore during chemical freeze-out. Here is when the standard Gondolo-Gelmini treatment fails to describe the decoupling process correctly and therefore fails to track the correct behaviour of the coupling constant λ as a function of the DM mass m_χ. In equations (4.33) and (4.34) the reduced efficiency of heat exchange processes is marked by a smaller value of the momentum transfer cross section γ.

A more detailed analysis can be done by plotting the evolution of the number density Y and the second statistical moment of the DM phase space distribution y (defined in (4.26) and related to the DM "temperature") at different values of x.

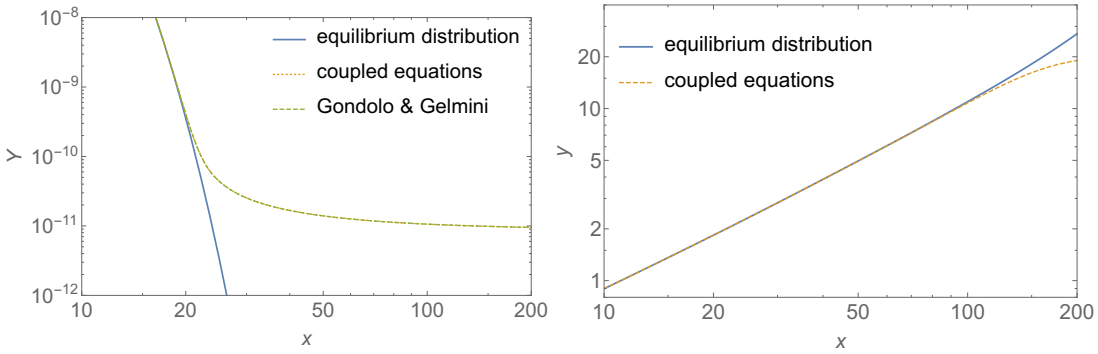

(a) Dimensionless number density as a function of x

(b) DM temperature parameter y as a function of x

Figure 6.4: $m_\chi = 45$ GeV

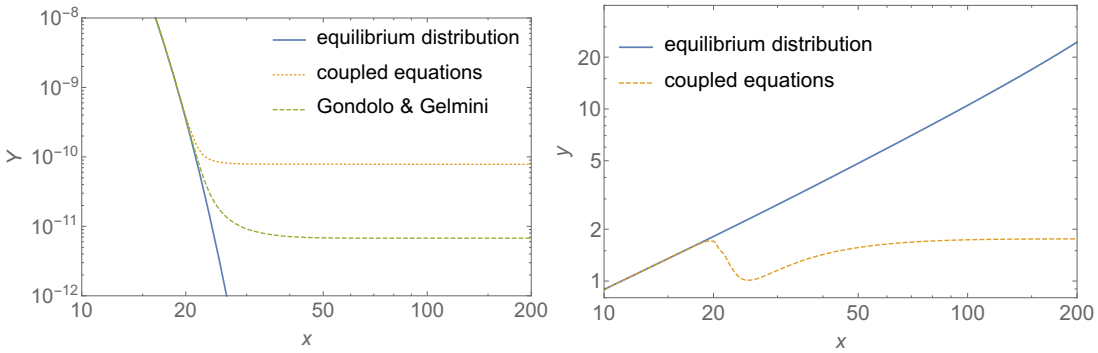

(a) Dimensionless number density as a function of x

(b) DM temperature parameter y as a function of x

Figure 6.5: $m_\chi = 58$ GeV

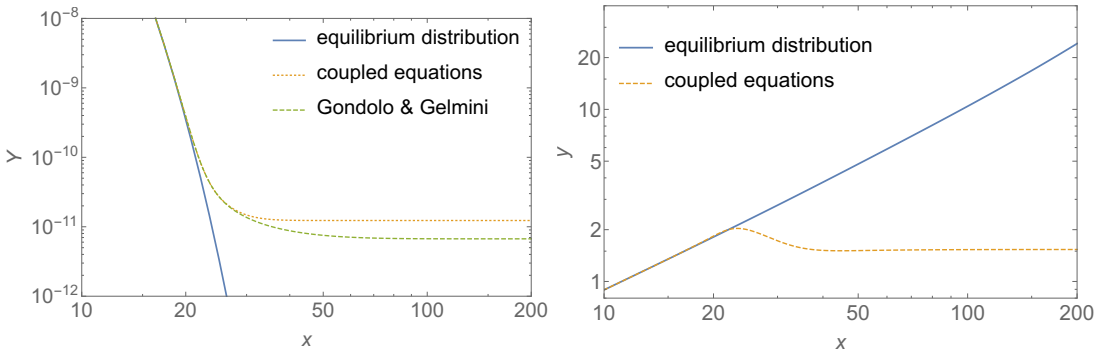

(a) Dimensionless number density as a function of x

(b) DM temperature parameter y as a function of x

Figure 6.6: $m_\chi = 60.5$ GeV

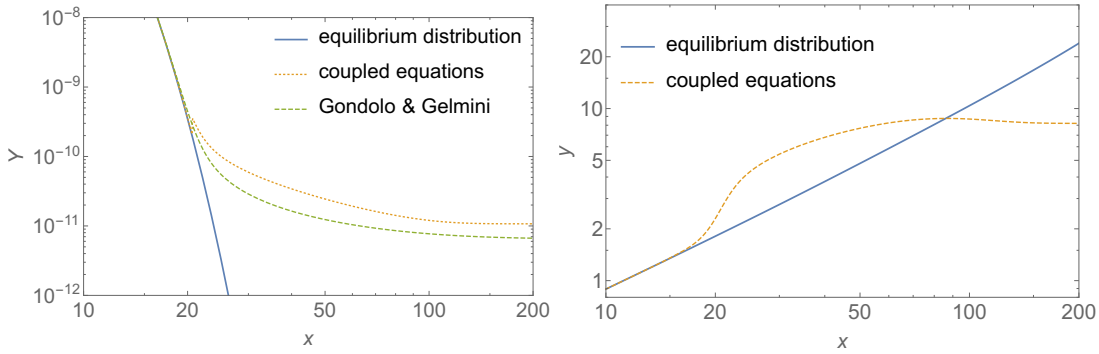

(a) Dimensionless number density as a function of x

(b) DM temperature parameter y as a function of x

Figure 6.7: $m_\chi = 62$ GeV

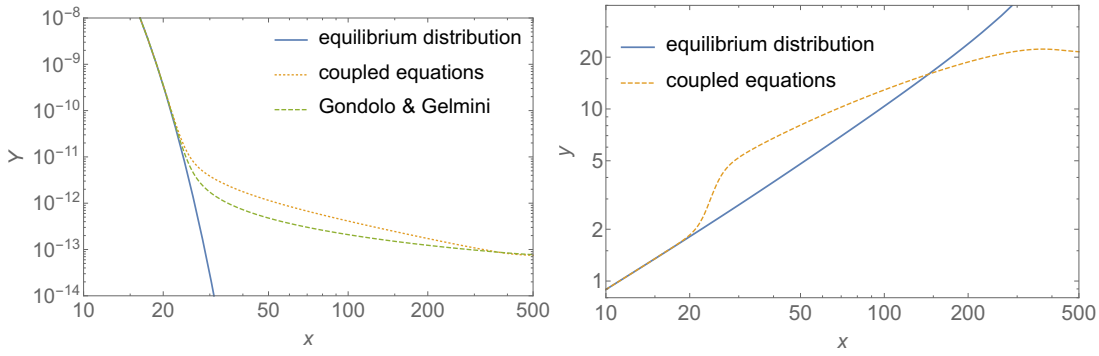

(a) Dimensionless number density as a function of x

(b) DM temperature parameter y as a function of x

Figure 6.8: $m_\chi = 62.5$ GeV

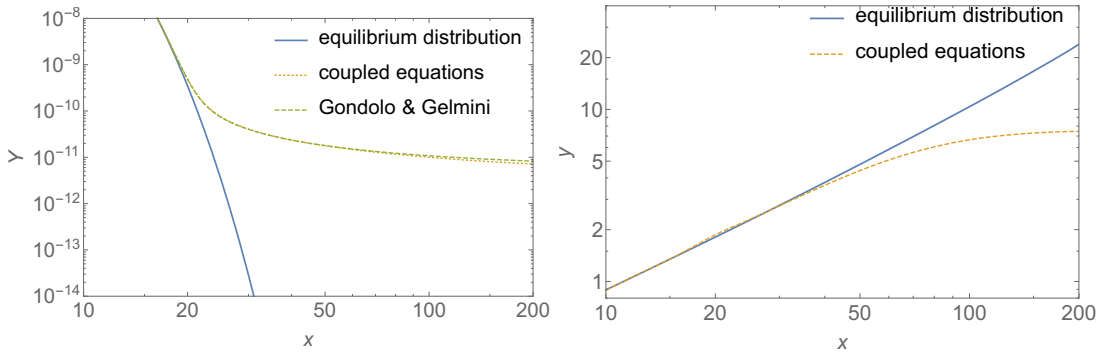

(a) Dimensionless number density as a function of x

(b) DM temperature parameter y as a function of x

Figure 6.9: $m_\chi = 63$ GeV

Starting with fig.(6.4) ($m_\chi = 45$ GeV), we see that this parameter point is sufficiently distant from the Higgs resonance, so the evolution of Y(x) resulting from the coupled equations is in very good agreement with the standard Gondolo Gelmini calculations. Here kinetic decoupling (marked by a deviation of the DM temperature parameter y from the equilibrium value, which is the value if y DM would have if still in thermal equilibrium the heat bath) takes place after $x \approx 100$, i.e. well after chemical decoupling (marked by a deviation of the number density from the equilibrium value).

Moving on to (6.5) ($m_\chi = 58$ GeV), we see that it is here particularly evident how the assumption of thermal equilibrium during chemical freeze-out cannot be assumed, resulting in the standard procedure failing to predict the correct evolution of the number density. The sudden decrease in y is a symptom of a different phase space distribution in the momentum space. This results in an earlier decoupling for Y and in a higher value for the relic density. This regime has described as "sub-resonant" in [2]. In contrast to what happens at $m_\chi = 45$ GeV, here kinetic and chemical decoupling take place at the same time.

The plots (6.6) ($m_\chi = 60.5$ GeV) show features which are similar to the ones showed in the previous couple of graphs, but now in a more attenuated way. More specifically, the DM temperature parameter y deviates from its equilibrium value at slightly later times compared to the previous paremeter point, resulting in a smaller deviation of the number density from its usual value.

At $m_\chi = 62$ GeV (fig. (6.7)) the evolution of the DM temperature parameter y is opposite compared to the parameter point $m_\chi = 58$ GeV, as it grows above its equilibrium value after decoupling. This regime has been described as "resonant" in [2].

The parameter point $m_\chi = 62.5$ (fig. (6.8)) is extremely close to the Higgs resonance, where $\chi\chi \to H$ annihilations are extremely enhanced and a much lower coupling constant λ is needed to obtain the correct relic density. Here the final relic density is not affected as much as in the previous parameter point by the simplistic assumption that thermal equilibrium is maintained during chemical freeze out, however the intermediate number density is noticeably affected, as the DM temperature parameter y deviates from its equilibrium value as quickly as in the previous cases.

Finally, the last plots (6.9), relative to $m_\chi = 63$ GeV show a similar behaviour to $m_\chi = 45$ GeV as these parameter points are sufficiently distant from the Higgs resonance, that the evolution of Y(x) resulting from the coupled equations are in very good agreement with the standard Gondolo Gelmini calculations. Again, kinetic decoupling takes place well after chemical decoupling.

To investigate better the difference between the "subresonant" and "resonant" regimes, here is plotted the ratio between the two thermal averages $\frac{\langle\sigma v\rangle}{\langle\sigma v\rangle_2}$ for $m_\chi = 58$ GeV and $m_\chi = 62$ GeV.

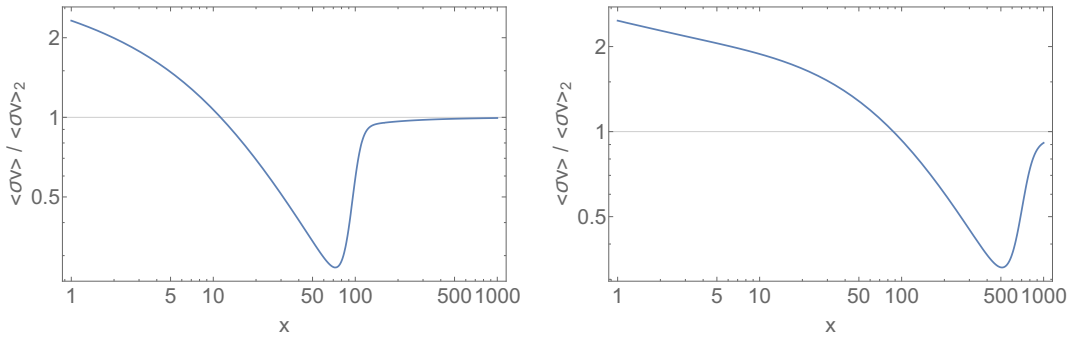

(a) $\frac{\langle\sigma v\rangle}{\langle\sigma v\rangle_2}$ at $m_\chi = 58$ GeV. **(b)** $\frac{\langle\sigma v\rangle}{\langle\sigma v\rangle_2}$ at $m_\chi = 62$ GeV.

Figure 6.10: $\frac{\langle\sigma v\rangle}{\langle\sigma v\rangle_2}$ for $m_\chi = 58$ GeV and $m_\chi = 62$ GeV.

Looking to fig. (6.10a) we see that here $\langle\sigma v\rangle < \langle\sigma v\rangle_2$ during the whole freeze - out process, which makes y decrease after the decoupling (see fig. (6.5)) as the term $\frac{sY}{x\tilde{H}}\left[\langle\sigma v\rangle_{neq} - \langle\sigma v\rangle_{2,neq}\right]$ in (4.34) becomes negative and large in absolute value.

On the other hand, looking to (6.10b) we see that here $\langle\sigma v\rangle > \langle\sigma v\rangle_2$ in the first part of the chemical decoupling but $\langle\sigma v\rangle > \langle\sigma v\rangle_2$ in a region where the number density of DM is still changing [1].

This results in y increasing above the equilibrium value immediately after kinetic decoupling, but decreasing below its equilibrium value afterwards x (see fig. (6.7)).

In conclusion, the effect of the generalized approach to relic density calculations implemented here in clearly visible. The analysis here can be compared with [2], where a similar analysis is conducted with identical results.

6.2 Self-Interacting Dark Matter

Here the improved way of computing relic density calculations is applied to a particle physics model where DM experiences a significant amount of self-interaction. As described in subsection 4.2.1, this class of models alleviate the most pressing discrepancies between observations and predictions of standard cosmology.

[1] Even if most of the change in Y happens before $x \approx 90$, which is when $\langle\sigma v\rangle = \langle\sigma v\rangle_2$, the quantities $\langle\sigma v\rangle_{neq}$ and $\langle\sigma v\rangle_{2,neq}$ are computed at later x than the canonical thermal averages when $y \neq y_{eq}$.

6.2.1 Theoretical background

Following [53], we describe non relativistic DM scattering with a Yukawa potential

$$V(r) = \frac{\alpha e^{-r m_{med}}}{r}, \tag{6.8}$$

arising from the interaction Lagrangian

$$\mathcal{L}_{int} = g_\chi \bar{\chi} \chi \phi. \tag{6.9}$$

Although the Schrödinger equation cannot be solved analytically for the Yukawa potential in the non-perturbative regime, a useful proxy is provided by the Hultéhn potential [53]:

$$V(r) = \pm \frac{\alpha \delta e^{-\delta r}}{1 - e^{-\delta r}}, \tag{6.10}$$

where the Hultéhn screening mass δ is defined as $\delta = \kappa m_{med}$ where κ is a numerical constant of order unity. We notice that the Yukawa and the Hulthéhn potentials behave similarly, scaling as $1/r$ at short distances and becoming screened for large distances [53].

The annihilation cross section at tree-level is [53]

$$\sigma v = \frac{3}{4} \frac{\pi \alpha^2}{m_\chi^2} v^2 \sqrt{1 - \frac{m_\phi^2}{m_\chi^2}}, \tag{6.11}$$

which can be rewritten as

$$\sigma v = 3 \frac{g_\chi^4}{64\pi} \frac{v^2}{m_\chi^2} \sqrt{1 - \frac{m_\phi^2}{m_\chi^2}}, \tag{6.12}$$

with $\alpha = \frac{g_\chi^2}{4\pi}$, in analogy with the standard fine structure constant for electromagnetic interactions.

In DarkSUSY, it has been preferred to use the following correction to (6.12) instead:

$$\sigma v = 3 g_\chi^4 \frac{p^4(-2m_\chi^6 + 10 m_\phi^4 m_\chi^2 - 17 m_\phi m_\chi^4 + 9 m_\chi^6)}{6\pi m_\chi (m_\phi^2 - 2m_\chi^2)^4} \sqrt{1 - \frac{m_\phi^2}{m_\chi^2}}. \tag{6.13}$$

Sommerfeld-enhanced DM annihilation

The most important feature of this particle physics module for our purposes is that being DM annihilation to scalar mediators a p-wave process [53], certain combinations of mediators mass m_{med}, DM mass m_χ and coupling constant α lead to Sommerfeld enhancements for DM annihilation [2] [73, 74].

[2] For a more detailed discussion of the Sommerfeld effect, see Appendix A

In other words, if $m_{med} \ll m_\chi$ the exchange of light mediators generates a potential that modifies the wave function of the DM particles, leading to an enhancement of the DM annihilation cross section at small velocities [3] which can be parametrized as follows:

$$\sigma v = S(v)(\sigma v)_0. \tag{6.14}$$

The Sommerfeld factor has been calculated analytically by means of approximation (6.9) for the potential, obtaining the following result for the Sommerfeld factor [75]:

$$S = \frac{2\pi\alpha \sinh(\frac{6m_\chi v}{\pi m_{med}})}{v\left[-\cos 2\pi\sqrt{\frac{6m_\chi\alpha}{\pi^2 m_{med}} - \frac{9m_\chi^2 v^2}{\pi^4 m_{med}^2}}\right) + \cosh\left(\frac{6m_\chi v}{\pi m_{med}}\right)\Bigg]}. \tag{6.15}$$

In the limit of small velocities, one finds that the denominator becomes very small if

$$m_{med} \approx \frac{6m_\chi\alpha}{\pi^2 n^2}, \tag{6.16}$$

for some integer n [75].

We can define how close is a parameter point (defined by a triplet of values for m_{med}, m_χ and α) to a resonance by defining the parameter

$$\delta = \left|\frac{m_{med} - m_{med}^{(n)}}{m_{med}^{(n)}}\right| = \left|1 - \frac{\pi^2 n^2 m_{med}}{6m_\chi\alpha}\right|. \tag{6.17}$$

If $\delta \ll \frac{1}{n\pi}$, i.e. when a parameter point is sufficiently close to a resonance, the Sommerfeld factor can be approximated as follows for low velocities ($v \ll \frac{\alpha}{n^2\pi}$):

$$S(v) = \frac{4\alpha^2}{n^2 v^2 + \alpha^2\delta^2}, \tag{6.18}$$

i.e. the Sommerfeld factor grows as $\frac{1}{v^2}$ until $v \lesssim v_{sat} = \frac{\alpha}{n}$, after which S saturates at $S \approx \frac{4}{\delta^2}$ [75] [4].

[3] The Sommerfeld enhancement only affects annihilation processes and not the scattering ones as it is originated by DM self-interaction potential facilitating and enforcing the interaction between two DM particles. This SIDM model doesn't include any DM-SM potential.

[4] Actually, this simplistic approach to compute the Sommerfeld factor can make it so large to have a annihilation cross section violating unitarity for very small velocities. Following [76] a modified Sommerfeld factor can be defined as follows: $S(v) = \frac{4\alpha^2}{n^2(v+v_c)^2+\alpha^2\delta^2}$ with $v_c = \frac{\alpha^4}{4n^2}$.

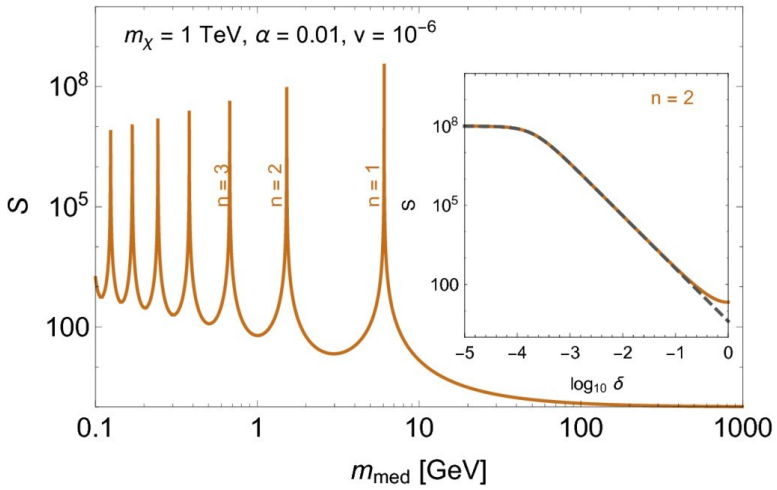

Figure 6.11: Sommerfeld enhancement factor S plotted against m_{med} for fixed values of m_χ, α and v. S shows a very large enhancement when the condition (6.16). The inset shows a zoom of the resonance marked by n=2 where S is plotted against δ (defined as (6.17)) [75]

It can be shown [5] that a power dependency for σv as $\sigma v = \sigma_0 v^{2n}$ results in a thermal average scaling as

$$\langle \sigma v \rangle_{eq} \simeq \sigma_0 x^{-n}. \tag{6.19}$$

A similar dependence holds for $\langle \sigma v \rangle_2$, according to

$$\frac{\langle \sigma v \rangle_2}{\langle \sigma v \rangle} = 1 + \frac{n}{3}. \tag{6.20}$$

Before kinetic decoupling, T_χ follows the heath bath temperature, therefore $y = y_{eq}$. This results in two different relations between v and x before and after kinetic decoupling; $v \propto x^{-\frac{1}{2}}$ before kinetic decoupling and $v \propto x^{-1}$ afterwards. As a consequence, we expect the thermal averaged cross section to behave as: $\langle \sigma v \rangle \propto x^{-\tilde{n}}$ where the exponent $\tilde{n}$ is

$$\tilde{n} = \begin{cases} \text{n} & \text{for x} \lesssim x_{kd} \\ \text{2n} & \text{for x} \gtrsim x_{kd}. \end{cases} \tag{6.21}$$

To understand how this affects DM relic density, we can as a first approach consider the single equation describing the 0-th moment of the Boltzmann equation

$$\frac{Y'}{Y} = -\left(1 - \frac{x}{3}\frac{g_*' s}{g_* s}\right)\frac{n_\chi \langle \sigma v \rangle_{eq}}{Hx}\left(1 - \frac{Y_{eq}^2}{Y^2}\right). \tag{6.22}$$

In a simplistic picture where $x_{kd} \gg x_{x_{cd}}$ around and after kinetic decoupling we have $Y \gg Y_{eq}$, therefore the solution to (6.22) is

$$Y(x)^{-1} = Y(x_i)^{-1} + \int_{x_i}^{x}\left(1 - \frac{x}{3}\frac{g_*' s}{g_* s}\right)\frac{s\langle \sigma v_{rel} \rangle}{Hx} dx, \tag{6.23}$$

for $x_i \gg x_{cd}$.

Using the relation $\langle \sigma v_{rel} \rangle \propto x^{-\tilde{n}}$ we find

$$Y(x)^{-1} - Y(x_i)^{-1} \simeq \lambda \begin{cases} \frac{1}{1+\tilde{n}} \left(\frac{1}{x_i^{1+\tilde{n}}} - \frac{1}{x^{1+\tilde{n}}} \right) & \text{for } \tilde{n} \neq \text{-1} \\ \ln(\frac{x}{x_i}) & \text{for } \tilde{n} = \text{-1.} \end{cases} \tag{6.24}$$

A noticeable change in Y for $x > x_1$ is only possible for $\tilde{n} \leq -1$. For the standard scenario, this condition is impossible to satisfy, as $\tilde{n} = 0$ for s-wave annihilation and $\tilde{n} = 1$ for the p-wave. However, a Sommerfeld-like enhancement of s-wave [5] annihilations is characterized by $\langle \sigma v_{rel} \rangle \propto v^{-2}$, i.e. $\tilde{n} = -2$ [5] [6].

Assuming again $\sigma v_{rel} \propto v^{2n}$ for the coupled system of differential equations instead, we find

$$\frac{y'}{y} \simeq \frac{n}{3} \frac{Y'}{Y} = \frac{\tilde{n}}{6} \frac{Y'}{Y}. \tag{6.25}$$

For $n < 0$, a decreasing Y will increase y even after kinetic decoupling.

6.2.2 Outcome

As there are three independent input parameters in this model, the DM particle mass m_χ, the mediator mass m_{med} and the coupling constant α, a more complicated search must be performed to obtain triplets of parameters such that the relic density is correct compared to the scalar singlet model. This is already implemented in DarkSUSY, where a search on the value of α is performed for each fixed couple of values for m_χ and m_{med}, then the mediator mass is changed and the search for the value of α procedure is repeated. Once covered a large range of values of m_{med}, m_χ is changed too and the whole procedure is repeated again.

In order to observe a second period of annihilation, the condition (6.16) has to be fulfilled. Therefore a list of parameter points (i.e. triplets of values m_χ, m_{med} and α) provided by the standard DarkSUSY SIDM routines such that the relic density is correct has been ordered according to how close the quantity n is to an integer number, according to relation (6.16). In order to maximize the resonant effect, the closest parameter point to the resonance marked by $n = 1$ has been chosen as this is the reonance with the biggest Sommerfeld enhancement factor S (see fig. (6.11)). The plots presented below are relative to the parameter point defined by $m_\chi = 18.66$ GeV, $m_{med} = 0.03141$ GeV, $\alpha = 0.002768$, for which the condition (6.16) is fulfilled with $n = 1$.

Before diving into the final results, the behaviour of the two thermal averages $\langle \sigma v \rangle$ and $\langle \sigma v \rangle_2$ has been studied, hoping to verify the relations (6.19), (6.20).

[5] See Appendix B for a more detailed discussion of p-waves and s-waves

[6] The relation $\langle \sigma v \rangle \propto v^{-2}$ only holds in the vicinities of a resonance; the behaviour of $\langle \sigma v \rangle$ is generally $\langle \sigma v \rangle \propto v^{-1}$.

The plot below shows the quantities $\langle\sigma v\rangle/x$ and $\langle\sigma v\rangle_2/x$, expecting a flat line at very low velocities (i.e. at very late times) if the thermal averages grow according to $\langle\sigma v\rangle \propto x$, $\langle\sigma v\rangle_2 \propto x$ after $x \approx 10^7$.

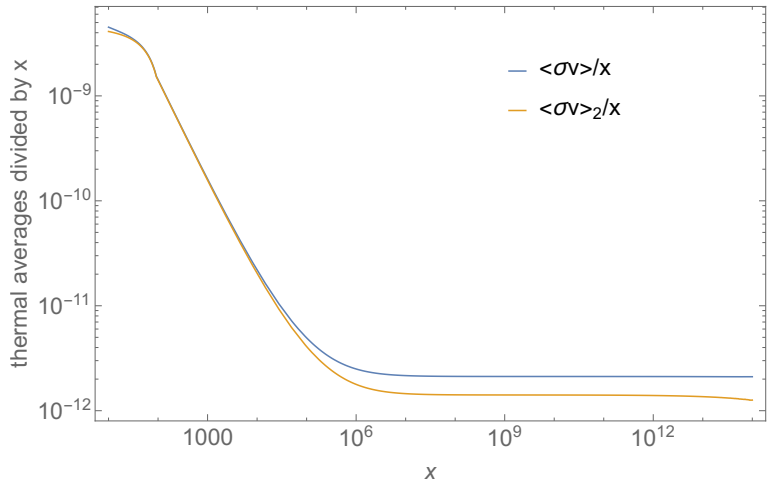

Figure 6.12: Here are plotted $\langle\sigma v\rangle/x$ and $\langle\sigma v\rangle_2/x$ as functions of x. The linear dependency of the thermal averages on x after $x \approx 10^7$ is well visible.

It is clear now how the thermal averages grow linearly in x after $x \approx 10^7$, according to (6.19) with $n = -1$, which is equivalent to $\langle\sigma v\rangle \propto v^{-2}$, $\langle\sigma v\rangle_2 \propto v^{-2}$.

In order to verify (6.20), the ratio $\frac{\langle\sigma v\rangle_2}{\langle\sigma v\rangle}$ has been plotted for a wide range of x, expecting to obtain a value of $\frac{2}{3}$.

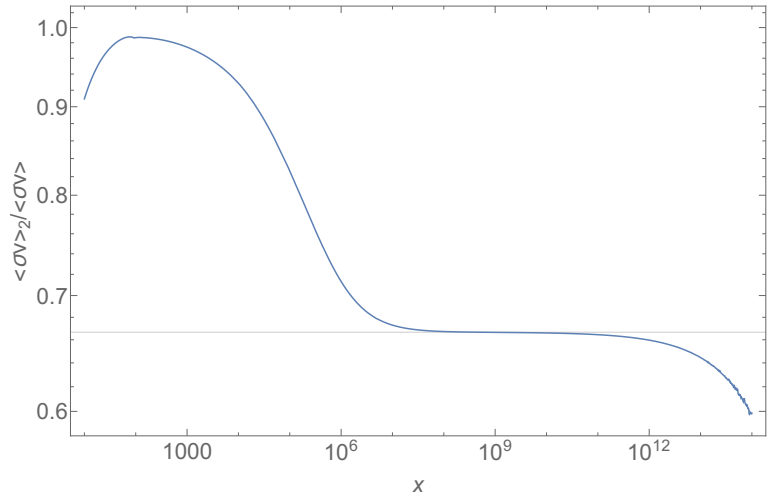

Figure 6.13: Ratio between $\langle\sigma v\rangle_2$ and $\langle\sigma v\rangle$ as function of x. The expected value of $\frac{2}{3}$ is marked with an horizontal solid line.

A plot of the ratio of these two quantities shows that (6.20) is correct between

$x \approx 10^7$ and $x \approx 10^{11}$, also indicating that $n = -1$ in this regime.

We can now move on to the final results. Similarly to what done for the scalar singlet model, the evolution of the dimensionless number density Y and the DM temperature parameter y has been plotted, the former in comparison with its evolution according to the standard Gondolo-Gelmini calculations and the latter in comparison with its equilibrium value y_{eq}.

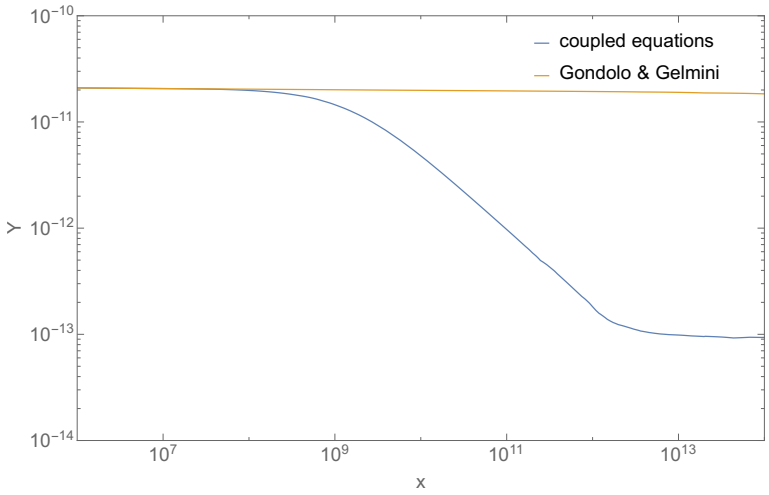

Figure 6.14: Evolution of the DM number density. A second period of annihilation where the umber density decreases by about two orders of magnitude is clearly visible.

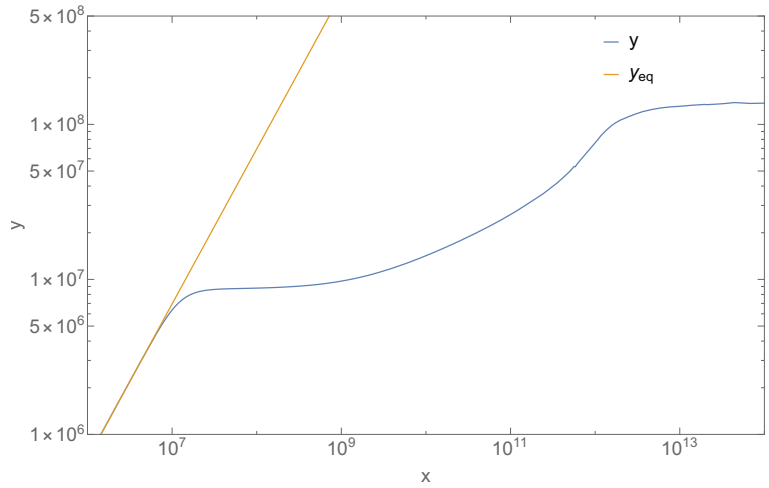

Figure 6.15: Evolution of the DM temperature parameter y

In particular, Fig. (6.14) shows a striking difference with respect to the uncoupled Boltzmann equations after $x \approx 10^7$, after which the WIMP annihilations decrease the relic density by more than two orders of magnitude until

the Sommerfeld enhancement saturates around $x \approx 10^{13}$. It can be noticed that this second period of annihilation takes place so late to continue after matter-radiation equality, which happens at about $x \approx 2 \times 10^{12}$ [5]. Taking this in account in the calculations (which includes redefining the Hubble rate H to also take in account the matter contribution, while in its current implementation it only includes the radiation term) might slightly improve the results, but not in a relevant way, as only a tiny fraction of the annihilation processes takes place after matter-radiation equality. Both plots show a behavior similar to that shown in fig. 4 in [5]. We cannot expect the plots to be exactly identical due to the dependency of Sommerfeld enhancement on the distance from the resonance (6.16) and the slightly different particle physics models.

As expected, the DM temperature parameter y departs from its equilibrium value roughly after $x \approx 10^7$, i.e. when the two thermal averages $\langle \sigma v \rangle$ and $\langle \sigma v \rangle_2$ fully enter the regime defined by (6.12) and when their ratio follows the relation

$$\frac{\langle \sigma v \rangle_2}{\langle \sigma v \rangle} = 1 + \frac{n}{3}. \tag{6.26}$$

(see fig. (6.13)).

We can understand how the Sommerfeld enhancement enters the coupled equations (4.33), (4.34) as follows: the two thermal averages $\langle \sigma v \rangle$ and $\langle \sigma v \rangle_2$ grow linearly well after the usual chemical and thermal decouplings. At around $x \approx 10^7$ the prefactor $\frac{\gamma(T)}{x\tilde{H}}$ in front of $\frac{y_{eq}}{y} - 1$ in eq. (4.34) becames vanishingly small, so the DM temperature parameter y stops being equal to y_{eq} and becomes constant. This corresponds to $T_\chi \propto a^{-2}$ [5], i.e. the usual scaling for non relativistic particles. The DM temperature parameter y enters eq. (4.33) only via the non equilibrium thermal average $\langle \sigma v \rangle_{neq}$, which is defined as the usual thermal average $\langle \sigma v \rangle$, evaluated at $T = ys^{\frac{2}{3}}/m_\chi$ instead of the usual $T = \frac{m_\chi}{x}$. When $y = y_{eq}$, $\langle \sigma v \rangle_{neq}$ is evaluated at the usual temperature $T = \frac{m_\chi}{x}$, therefore $\langle \sigma v \rangle_{neq} = \langle \sigma v \rangle$. Here, however $y < y_{eq}$ (see fig. (6.15)), hence $\langle \sigma v \rangle_{neq}$ is evaluated at a lower temperature than usual(i.e. an higher x due to the definition $x = \frac{m_\chi}{T}$). As already mentioned, $\langle \sigma v \rangle$ grows linearly in x in this regime, so we have $\langle \sigma v \rangle_{neq} > \langle \sigma v \rangle$. Looking up to (4.33) we see that this has the effect of making the right-hand side of the differential equation negative, hence reducing the number density Y.

Chapter 7

Discussion

A remarkable feature of the improved way of computing the relic density of DM presented here is the fact that it results in a noticeable difference in the relic density in very different scenarios. The difference in the relic density reaches one order of magnitude in the scalar singlet model around $x = 58$ GeV (6.5) and exceeds two orders of magnitude in the SIDM model (6.14).

In both cases, the maximum effect is present in a peculiar situation. In the scalar singlet model a noticeable discrepancy appears in the vicinity of a resonance with the Higgs boson, when the process $\chi\chi \to H$ is strongly enhanced and a very low coupling constant λ is needed to get the correct relic density. Such a small coupling constant results in a small momentum transfer rate γ which makes the heat exchange processes less effective. As a result, thermal equilibrium is not maintained during freeze-out and the standard way of calculating the relic density fails as its value results to be about 10 times bigger than what resulting from standard calculations. Hence, in order to obtain the correct relic density, a bigger coupling constant λ by more than a factor of two is needed. The results are in good agreement with [2], where a similar analysis has been done.

In the SIDM model instead, due to Sommerfeld enhancement annihilation processes between DM and SM particles are strongly enhanced at low velocities, i.e. at late times. This phenomenon makes annihilation processes sufficiently strong for DM to enter a new era of annihilation. More specifically, the DM temperature parameter y stops following its equilibrium value y_{eq} around 10^7, and becomes constant. Due to the modified approach to relic density calculations and due to Sommerfeld enhancement, which makes the thermal averages scale as $\langle\sigma v\rangle \propto v^{-2}$,$\langle\sigma v\rangle_2 \propto v^{-2}$ at low velocities, this affects the evolution of the dimensionless number density Y, which decreases in the interval $10^8 \lesssim x \lesssim 10^{13}$. During this period, the DM number density is reduced by more than two orders of magnitude.

In both cases the code has proven to be fast (a factor of 10^3 faster than the analogous Mathematica script used for [2]) and reliable. A modified and optimized version of this code may be implemented in future versions of DS.

Chapter 8

Conclusion

This implementation of the improved way of computing the relic density according to [2] has proven to successfully capture a deviation from the results from standard calculations both in the scalar singlet and in the self interacting DM particle modules. For the former, the results can be compared with [2], where a similar analysis has been done on the same particle model, with very similar results. Moreover, the current implementation within DarkSUSY (and therefore written in Fortran) has proven to be about three orders of magnitude faster than the Mathematica script used for the mentioned article, hence allowing for more complex scans in a relatively short time in the future. The latter, instead has little literature background, so we can only stress how noticeable this effect (as the relic density is reduced by more than two orders of magnitude during the second period of annihilation experienced by DM) and mention that more extensive scans on the parameter space are planned for the future. This is because the parameter point for this theory is defined by a triplet of values m_χ, m_{med}, α, so the impact of the calculations on the correct values in order to obtain the correct relic density is less direct and requires a more complex analysis than the scalar singlet model.

As pointed out by [5], a second period of DM annihilations well after kinetic decoupling has an impact on structure formation as the DM velocity dispersion is affected at a time when structure formation is starting to take place. More specifically, the DM velocity dispersion can be related to a small-scale cutoff in the power spectrum of matter density fluctuations corresponding to the mass of the smallest gravitationally bound objects m_{cut} [77]. A detailed analysis of this effect is beyond the scope of this thesis but a function returning m_{cut} as a function of the temperature after kinetic decoupling already exists in DarkSUSY, so it is sufficient to use the asymptotic value of the DM temperature parameter y as computed in the improved treatment for relic density calculations computed here to obtain corrected values for m_{cut}.

We emphasize that the newest version of DarkSUSY allows the user to easily link in different particle physics modules, so this improved Boltzmann solver could

be used for different particle physics models in the future and more extensive and systematic scans of the parameter space for the SIDM model could also be carried. Once a part of the standard DarkSUSY core libraries, this package could allow an external user to easily link it to any particle physics module (including external-supplied ones, see fig. (5.1) and the DarkSUSY manual for reference [63]). Any particle physics model with a low scattering rate in certain regions of its parameter space or with a velocity-dependent scattering annihilation rate might be a good candidate to provide different results compared to standard Gondolo-Gelmini relic density calculations.

Appendix A

Sommerfeld effect

First introduced by Sommerfeld in 1931 [78], the Sommerfeld effect is an elementary effect in non relativistic quantum mechanics which describes how an interaction cross section is affected by the presence of a potential acting on the particles involved in the process. More specifically, this phenomenon takes the name of Sommerfeld enhancement.

Following [79], we make the following assumptions to describe the situation:

- The incident particle is a non relativistic free particle (without the added potential), therefore we can describe the incident particle with the wavefunction

$$\psi_k^{(0)}(\mathbf{x}) = e^{ikz}, \tag{A.1}$$

  if the particle moves along the z-axis.

- If the interaction is pointlike and takes place only in the origin, the interaction cross section is proportional to the squared wavefunction in the origin as the latter can be interpreted as the probability that a particle is located there. As in our case we want to include a potential and hence a non-pointlike but still spatially limited interaction (extending up to a radius r_0 with $0 < r_0 \ll 1$), we can easily extend this result.

- The added potential has central symmetry, i.e. its magnitude only depends on the distance from the origin. Therefore we have that the scattering of a central potential results in outgoing spherical waves of the form

$$\psi_k \to e^{ikz} + f(\theta)\frac{e^{ikr}}{r} \textbf{as } \mathbf{r} \to \infty. \tag{A.2}$$

  The Sommerfeld enhancement factor S is defined as

$$\sigma = \sigma_0 S, \tag{A.3}$$

and is the case of a pointlike interaction equal to

$$S = \frac{|\psi_k(0)|^2}{\left|\psi_k^{(0)}(0)\right|^2} = |\psi_k(0)|, \tag{A.4}$$

while in the case of a not pointlike but still spatially limited interaction it can be approximated to:

$$S = \frac{\int_0^{r_0} |\psi_k(r)|^2}{\int_0^{r_0} |\psi_k^{(0)}(r)|^2 dr}, \tag{A.5}$$

so we need to solve the Schrödinger equation to find the wavefunction $\psi_k(0)$.

Generally, axially symmetric solutions of the Schrödinger equation for the wavefunction (A.2) are of the form

$$\psi_{kl} = \sum_{l=0}^{\infty} A_l P_l(\cos(\theta)) R_{kl}(r), \tag{A.6}$$

where A_l is a parameter to be determined, $P_l((\theta))$ are the associated Legendre functions and $R_{kl}(r)$ is the radial part of the wavefunction. As we assumed a central potential, the angle-dependent parameter A_l is independent of the potential and takes the standard form $\frac{i^l e^{i\delta_l}(2l+1)}{k}$.

The interaction modelling DM self-interaction is the Yukawa potential, which generalizes the Coulomb potential in the case of massive force carriers. There is no analytical solution to the Schrödinger equation with this kind of interaction. However, several numeric implementations of this problem are available in the literature [80, 81], thanks to a renewed interest in the subject due to its relevance in DM theories.

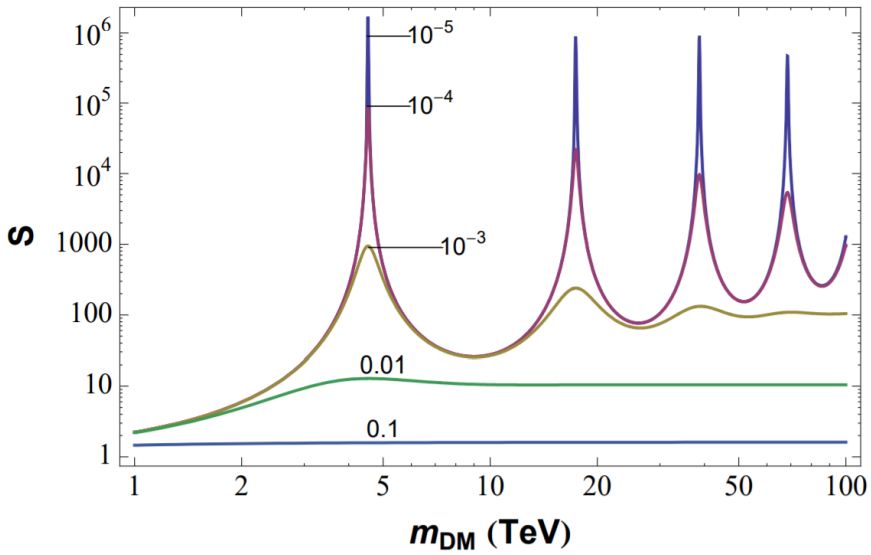

Figure A.1: The Sommerfeld enhancement factor S as a function of the mass of the scattering particles (here already assumed to be a DM particle) for different values of the velocity (expressed as a fraction of the speed of light c), from 10^{-5} 10^{-1}. This figure, taken from [81], is relative to a boson mass equal to 90 GeV and a gauge coupling $\alpha = \frac{1}{30}$, values corresponding to an exchange of Z bosons

We notice that for very low velocities the Sommerfeld enhancement factor S can reach extremely high values close to the resonances, of the order of 10^6.

Appendix B

Partial wave analysis

The Schrödinger equation for a spherically symmetrical potential V(r) admits the separable solutions

$$\psi(r,\theta,\phi) = R(r)Y_l^m(\theta,\phi), \tag{B.1}$$

where Y_l^m is a spherical harmonic, and u(r) = rR(r) satisfies the equation:

$$-\frac{h^2}{2m}\frac{d^2u}{dr^2} + \left[V(r) + \frac{h^2}{2m}\frac{l(l+1)}{r^2}\right]u = Eu. \tag{B.2}$$

At very large r the potential tends to zero, hence $\frac{d^2u}{dr^2} \approx -k^2u$, whose solution is of the form

$$u(r) = Ce^{ikr} + De^{-ikr}, \tag{B.3}$$

with the first term corresponding to an incoming wave. However, a more sensible approximation valid for an intermediate region located between the "radiation zone" and the close vicinities of the actual scattering region consists in neglecting V but not the centrifugal term.

In this case the radial equation becomes

$$\frac{d^2u}{dr^2} - \frac{l(l+1)}{r^2}u = -k^2u, \tag{B.4}$$

and the general solution is a linear combination of spherical Bessel functions:

$$u(r) = Arj_l(kr) + Brn_l(kr). \tag{B.5}$$

However, in order to attribute a physical meaning to different components of the wave it is necessary to rewrite the previous expression as a sum of the so called Hankel spherical harmonics:

$$h_l^{(1)}(x) = j_l(x) + in_l(x) \quad h_l^{(2)}(x) = j_l(x) - in_l(x). \tag{B.6}$$

At large r, the Hankel function of the first kind scales as e^{ikr}/r, whereas the Hankel function of the second kind scales as e^{-ikr}/r. For outgoing waves, then we need spherical Hankel functions of the first kind.

Outside the scattering region and where V=0 the wave function becomes

$$\psi(r,\theta,\phi) = A\Big\{e^{ikz} + \sum_{l,m} C_{l,m} h_l^{(1)}(kr) Y_l^m(\theta,\phi)\Big\}. \tag{B.7}$$

The first term describes the incident plane wave and the sum represents the scattered wave.

The term corresponding to the value l=0 is conventionally designated with the letter s while the term with l=1 corresponds to the letter p [1].

[1] See [82] for a more detailed analysis.

Appendix C

Møller velocity and laboratory velocity

The so called "Møller velocity" v_{mol}, defined as[83]:

$$v_{mol} = \sqrt{(v_1 + v_2)^2 - (v_1 \times v_2)^2}, \tag{C.1}$$

or alternatively as [2]

$$v_{mol} = \frac{\sqrt{(p_1 \cdot p_2)^2 - m_1^2 m_2^2}}{E_1 E_2}, \tag{C.2}$$

is not actually a velocity in the physical sense, as it does not transform according to the Lorentz transformations and only serves the purpose of simplifying the notation in the thermal average [83]. As pointed out in [83], the velocity appearing in the definition of thermal average $\langle \sigma v \rangle$ is actually the Møller velocity:

$$\langle \sigma v \rangle = \frac{\int d^3\mathbf{p}_1 d^3\mathbf{p}_2 e^{-E_1/T} e^{-E_2/T} \sigma v_{mol}}{\int d^3\mathbf{p}_1 d^3\mathbf{p}_2 e^{-E_1/T} e^{-E_2/T}}. \tag{C.3}$$

This expression was shown to be equal to the single integral (4.19):

$$\begin{aligned} \langle \sigma v \rangle = \frac{g_\chi^2}{n_{\chi,eq}^2} \int \frac{d^3p}{(2\pi)^3} \frac{d^3\tilde{p}}{(2\pi)^3} \sigma v_{\bar{\chi}\chi \to \bar{f}f} f_{\chi,eq}(p) f_{\chi,eq}(\bar{p}) = \\ \int_1^\infty d\tilde{s} \sigma_{\bar{\chi}\chi \to \bar{f}f} v_{lab} \frac{2m_\chi \sqrt{\tilde{s}-1} K_1(\frac{2\sqrt{\tilde{s}} m_\chi}{T})}{T K_2^2(\frac{m_\chi}{T})}, \end{aligned} \tag{C.4}$$

in the Gondolo-Gelmini paper [1], where the velocity v_{rel} is present instead.

However, it can be shown that in the laboratory frame (i.e. where one of the DM particles is at rest) the two velocities v_{mol} and v_{rel} are equal.

Starting from the definition $v_{Møl} = \frac{\sqrt{(\mathbf{p}_1 \cdot \mathbf{p}_1)^2 - m_\chi^4}}{E_1 E_2}$ and recalling that in the lab frame we have $\mathbf{p}_1 \cdot \mathbf{p}_2 = m\sqrt{m^2 + p^2}$ and $E_1 E_2 = m\sqrt{m^2 + p^2}$

$$v_{M\o l} = \frac{\sqrt{(m\sqrt{m^2+p^2})^2 - m^4}}{m\sqrt{m^2+p^2}} = \frac{p}{\sqrt{m^2+p^2}}. \tag{C.5}$$

As for v_{rel}, defined as $v_{lab} = \frac{\sqrt{s(s-4m_\chi^2)}}{s-2m_\chi^2}$, we evaluate the Mandelstam variable s in the lab frame as $s = (\mathbf{p}_1 + \mathbf{p}_2)^2 = 2(m^2 + m\sqrt{m^2+p^2})$, so

$$\begin{aligned} v_{lab} = \frac{\sqrt{(2m\sqrt{m^2+p^2}+2m^2)(2m\sqrt{m^2+p^2}-2m^2)}}{2m\sqrt{m^2+p^2}} = \\ \frac{4m^2(m^2+p^2)-4m^4}{2m\sqrt{m^2+p^2}} = \frac{p}{\sqrt{m^2+p^2}}, \end{aligned} \tag{C.6}$$

where $m = m_\chi$, $p_1 = 0$ and $p_2 = p$.

Therefore, $v_{M\o l} = v_{lab}$ in the laboratory reference frame. It is possible to show that this equality holds in all reference frames which are equivalent to applying a Lorentz boost to the pair of particles along the direction of the non zero momentum (p_2 in our notation).

Appendix D

Power series expansion of expression in $\langle \sigma v \rangle_2$

As mentioned in chapter (5), the expression for $\langle \sigma v \rangle_2$ (4.35) includes a factor, namely the term between square brackets in the integrand function in ϵ, which is constituted by the sum of two quantities which are opposite in sign and very close in absolute value, therefore an extremely high precision in the numerical computation of these quantities is required. For $x \gtrapprox 10^9$, the most significant range in $\tilde{s}$ and ϵ_+ is so close to 1 that the two quantities mentioned before have to be evaluated correctly at least to the 8th digit, a degree of precision which is not guaranteed in our case. Therefore, it has been necessary to expand the two addends $f_1(\epsilon_+, \tilde{s}) = \epsilon_+ \sqrt{(\tilde{s}-1)(\epsilon_+^2-1)}$ and $f_2(\epsilon_+, \tilde{s}) = \frac{1}{2\sqrt{\tilde{s}}} \log\left(\frac{\sqrt{\tilde{s}}\epsilon_+ - \sqrt{(\tilde{s}-1)(\epsilon_+^2-1)}}{\sqrt{\tilde{s}}\epsilon_+ + \sqrt{(\tilde{s}-1)(\epsilon_+^2-1)}} \right)$ in power series around $\tilde{s} = 1$ and $\epsilon_+ = 1$. To clearify the notation, we can define the distance from the center of the expansion as $r = \sqrt{(\epsilon_+ - 1)^2 + (\tilde{s}-1)^2}$.

At zeroth order we have:

$$f_1(\epsilon_+, \tilde{s}) = 0 + O(r) \tag{D.1}$$
$$f_2(\epsilon_+, \tilde{s}) = 0 + O(r). \tag{D.2}$$

Proceeding with the first order expansion,

$$f_1(\epsilon_+, \tilde{s}) = \sqrt{2(\tilde{s}-1)(\epsilon_+ - 1)} + O(r^2) \tag{D.3}$$
$$f_2(\epsilon_+, \tilde{s}) = -\sqrt{2(\tilde{s}-1)(\epsilon_+ - 1)} + O(r^2). \tag{D.4}$$

As expected, the lowest non-zero term is the same, but with an opposite sign for the two functions.

The next order expansion, however, allows us to capture the dominating con-

tribution to the sum of the two terms:

$$f_1(\epsilon_+, \tilde{s}) = \sqrt{2(\tilde{s}-1)(\epsilon_+ - 1)}\left(1 + \frac{5}{4}(\epsilon_+ - 1)\right) + O(r^3) \quad \text{(D.5)}$$

$$f_2(\epsilon_+, \tilde{s}) = -\sqrt{2(\tilde{s}-1)(\epsilon_+ - 1)}\left(1 - (\tilde{s}-1) - \frac{3}{4}(\epsilon_+ - 1)\right) + O(r^3), \quad \text{(D.6)}$$

therefore, the quantity we were looking for is

$$f_1(\epsilon_+, \tilde{s}) + f_2(\epsilon_+, \tilde{s}) = \sqrt{2(\tilde{s}-1)(\epsilon_+ - 1)}\left(2(\epsilon_+ - 1) + (\tilde{s}-1)\right) + O(r^3). \quad \text{(D.7)}$$

Here are some plots which help illustrating the situation. For all of them, only a region close to the central point of the expansion (namely, the region $\epsilon_+ \subset \{1, 1.01\}$, $\tilde{s} \subset \{1, 1.01\}$) is considered as in front of the term $f_1(\epsilon_+, \tilde{s}) + f_2(\epsilon_+, \tilde{s})$ a factor of $\exp\{-2\sqrt{\tilde{s}}x\epsilon_+\}$ is present in the integral, which suppresses the integrand function for higher values of ϵ_+ and $\tilde{s}$.

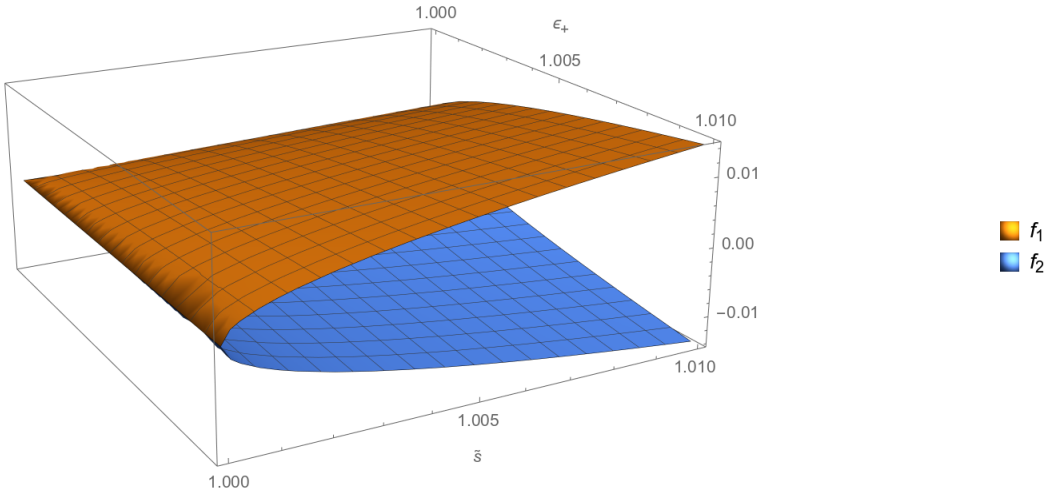

Figure D.1: $f_1(\epsilon_+, \tilde{s})$ and $f_2(\epsilon_+, \tilde{s})$ are both equal to 0 at $\epsilon_+ = 1$, $\tilde{s} = 1$ and show a similar behaviour elsewhere, apart from the opposite sign

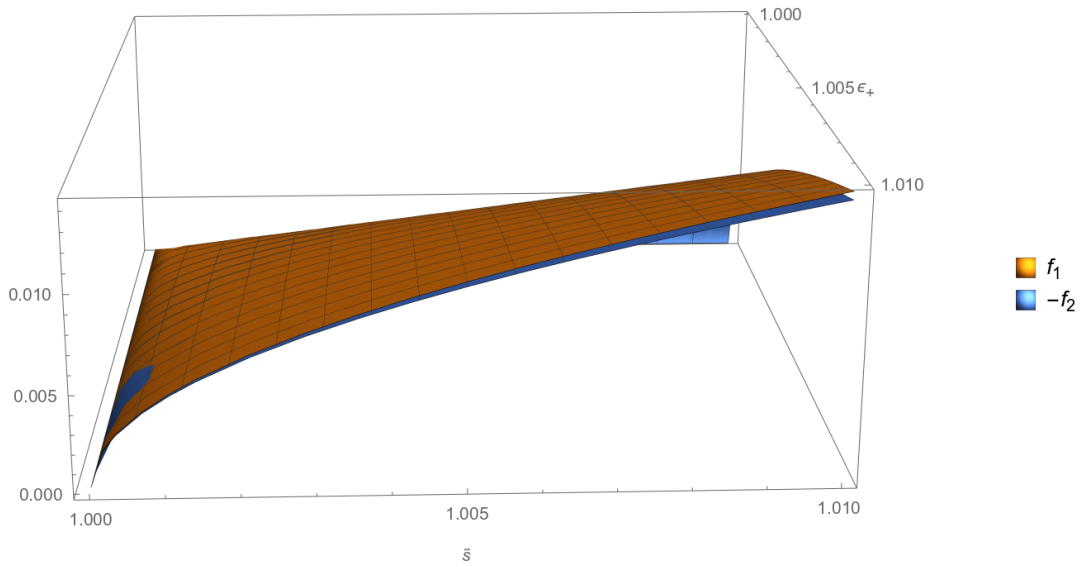

Figure D.2: To highlight how close $f_1(\epsilon_+, \tilde{s})$ and $f_2(\epsilon_+, \tilde{s})$ are in absolute value, $f_1(\epsilon_+, \tilde{s})$ and $-f_2(\epsilon_+, \tilde{s})$ have been plotted here. The difference between the two is only noticeable at the lower right corner of the picture, corresponding to $\epsilon_+ = 1.01$ and $\tilde{s} = 1.01$.

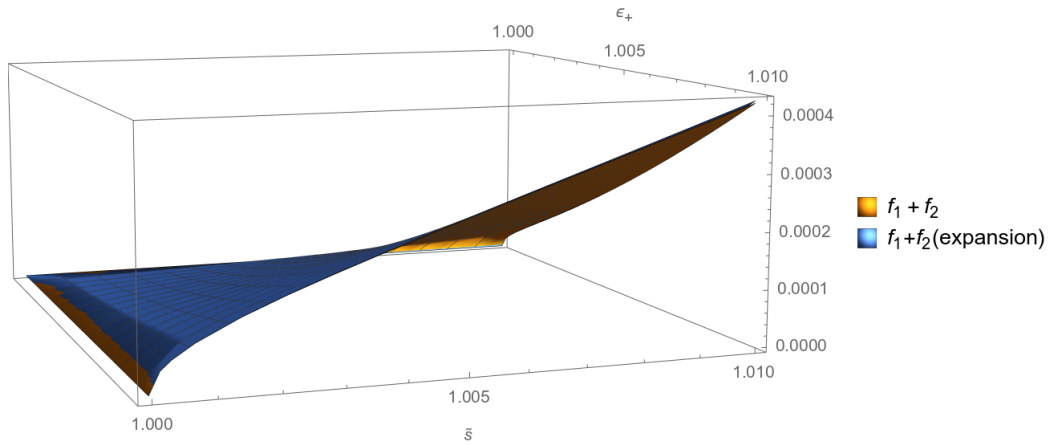

Figure D.3: Here is a comparison between $f_1(\epsilon_+, \tilde{s}) + f_2(\epsilon_+, \tilde{s})$, i.e. the actual function to be integrated, and the second-order approximation of the same quantity. The approximation follows the original function very well as the discrepancy between the two is not visually noticeable.

Bibliography

[1] Paolo Gondolo and Graciela Gelmini. "Cosmic abundances of stable particles: Improved analysis". In: *Nuclear Physics B* 360.1 (1991), pp. 145–179. ISSN: 0550-3213. DOI: https://doi.org/10.1016/0550-3213(91)90438-4. URL: http://www.sciencedirect.com/science/article/pii/0550321391904384.

[2] Tobias Binder et al. "Early kinetic decoupling of dark matter: when the standard way of calculating the thermal relic density fails". In: *Phys. Rev.* D96.11 (2017), p. 115010. DOI: 10.1103/PhysRevD.96.115010. arXiv: 1706.07433 [astro-ph.CO].

[3] Torsten Bringmann et al. "DarkSUSY 6 : An Advanced Tool to Compute Dark Matter Properties Numerically". In: (2018). arXiv: 1802.03399 [hep-ph].

[4] Laura G. van den Aarssen, Torsten Bringmann, and Christoph Pfrommer. "Is dark matter with long-range interactions a solution to all small-scale problems of $\Lambda CDM cosmology$?". In: *Phys. Rev. Lett.* 109 (2012), p. 231301. DOI: 10.1103/PhysRevLett.109.231301. arXiv: 1205.5809 [astro-ph.CO].

[5] Laura G. van den Aarssen, Torsten Bringmann, and Yasar C Goedecke. "Thermal decoupling and the smallest subhalo mass in dark matter models with Sommerfeld-enhanced annihilation rates". In: *Phys. Rev.* D85 (2012), p. 123512. DOI: 10.1103/PhysRevD.85.123512. arXiv: 1202.5456 [hep-ph].

[6] G. Bertone and D. Hooper. "A History of Dark Matter". In: *ArXiv e-prints* (May 2016). arXiv: 1605.04909.

[7] K. Freese. "Review of Observational Evidence for Dark Matter in the Universe and in upcoming searches for Dark Stars". In: *EAS Publications Series*. Ed. by E. Pécontal et al. Vol. 36. EAS Publications Series. 2009, pp. 113–126. DOI: 10.1051/eas/0936016. arXiv: 0812.4005.

[8] David N. Spergel. "The dark side of cosmology: Dark matter and dark energy". In: *Science* 347.6226 (2015), pp. 1100–1102. ISSN: 0036-8075. DOI: 10.1126/science.aaa0980. eprint: http://science.sciencemag.org/content/347/6226/1100.full.pdf. URL: http://science.sciencemag.org/content/347/6226/1100.

[9] D. Scott and G. F. Smoot. "Cosmic Microwave Background Mini-review". In: *ArXiv e-prints* (May 2010). arXiv: 1005.0555 [astro-ph.CO].

[10] Planck Collaboration et al. "Planck 2015 results. XVI. Isotropy and statistics of the CMB". In: 594, A16 (Sept. 2016), A16. DOI: 10.1051/0004-6361/201526681. arXiv: 1506.07135.

[11] J. R. Primack. "Dark Matter and Structure Formation in the Universe". In: *ArXiv Astrophysics e-prints* (July 1997). eprint: astro-ph/9707285.

[12] F. Zwicky. "Die Rotverschiebung von extragalaktischen Nebeln". In: *Helvetica Physica Acta* 6 (1933), pp. 110–127.

[13] S. van den Bergh. "The Early History of Dark Matter". In: 111 (June 1999), pp. 657–660. DOI: 10.1086/316369. eprint: astro-ph/9904251.

[14] V. C. Rubin and W. K. Ford Jr. "Rotation of the Andromeda Nebula from a Spectroscopic Survey of Emission Regions". In: 159 (Feb. 1970), p. 379. DOI: 10.1086/150317.

[15] D. Clowe et al. "A Direct Empirical Proof of the Existence of Dark Matter". In: 648 (Sept. 2006), pp. L109–L113. DOI: 10.1086/508162. eprint: astro-ph/0608407.

[16] De-Chang Dai, Reijiro Matsuo, and Glenn Starkman. "Gravitational Lenses in Generalized Einstein-Aether theory: The Bullet Cluster". In: *Phys. Rev.* D78 (2008), p. 104004. DOI: 10.1103/PhysRevD.78.104004. arXiv: 0806.4319 [gr-qc].

[17] Richard Massey, Thomas Kitching, and Johan Richard. "The dark matter of gravitational lensing". In: *Rept. Prog. Phys.* 73 (2010), p. 086901. DOI: 10.1088/0034-4885/73/8/086901. arXiv: 1001.1739 [astro-ph.CO].

[18] Debaprasad Maity and Pankaj Saha. "Connecting CMB anisotropy and cold dark matter phenomenology via reheating". In: (2018). arXiv: 1801.03059 [hep-ph].

[19] B. Carr, F. Kühnel, and M. Sandstad. "Primordial black holes as dark matter". In: 94.8, 083504 (Oct. 2016), p. 083504. DOI: 10.1103/PhysRevD.94.083504. arXiv: 1607.06077.

[20] P. Ivanov, P. Naselsky, and I. Novikov. "Inflation and primordial black holes as dark matter". In: *Phys. Rev. D* 50 (12 Dec. 1994), pp. 7173–7178. DOI: 10.1103/PhysRevD.50.7173. URL: https://link.aps.org/doi/10.1103/PhysRevD.50.7173.

[21] Ely D. Kovetz. "Probing Primordial-Black-Hole Dark Matter with Gravitational Waves". In: *Phys. Rev. Lett.* 119.13 (2017), p. 131301. DOI: 10.1103/PhysRevLett.119.131301. arXiv: 1705.09182 [astro-ph.CO].

[22] John Preskill, Mark B. Wise, and Frank Wilczek. "Cosmology of the Invisible Axion". In: *Phys. Lett.* B120 (1983). [,URL(1982)], pp. 127–132. DOI: 10.1016/0370-2693(83)90637-8.

[23] H.-C. Cheng, J. L. Feng, and K. T. Matchev. "Kaluza-Klein Dark Matter". In: *Physical Review Letters* 89.21, 211301 (Oct. 2002), p. 211301. DOI: 10.1103/PhysRevLett.89.211301. eprint: hep-ph/0207125.

[24] Edward W. Kolb and Richard Slansky. "Dimensional Reduction in the Early Universe: Where Have the Massive Particles Gone?" In: *Phys. Lett.* 135B (1984), p. 378. DOI: 10.1016/0370-2693(84)90298-3.

[25] F. Bezrukov, H. Hettmansperger, and M. Lindner. "keV sterile neutrino dark matter in gauge extensions of the standard model". In: 81.8, 085032 (Apr. 2010), p. 085032. DOI: 10.1103/PhysRevD.81.085032. arXiv: 0912.4415 [hep-ph].

[26] Gary Steigman and Michael S. Turner. "Cosmological constraints on the properties of weakly interacting massive particles". In: *Nuclear Physics B* 253 (1985), pp. 375–386. ISSN: 0550-3213. DOI: https://doi.org/10.1016/0550-3213(85)90537-1. URL: http://www.sciencedirect.com/science/article/pii/0550321385905371.

[27] Edward W. Kolb and Michael S. Turner. "The Early Universe". In: *Front. Phys.* 69 (1990), pp. 1–547.

[28] Kelvin K. S. Wu, Ofer Lahav, and Martin J. Rees. "The large-scale smoothness of the Universe". In: *Nature* 397 (1999). [,19(1998)], pp. 225–230. DOI: 10.1038/16637. arXiv: astro-ph/9804062 [astro-ph].

[29] J. C. Jackson. "Ultra-compact radio sources and the isotropy and homogeneity of the Universe". In: 426 (Oct. 2012), pp. 779–783. DOI: 10.1111/j.1365-2966.2012.21734.x. arXiv: 1207.0697.

[30] P. A. R. Ade et al. "Planck 2015 results. XIII. Cosmological parameters". In: *Astron. Astrophys.* 594 (2016), A13. DOI: 10.1051/0004-6361/201525830. arXiv: 1502.01589 [astro-ph.CO].

[31] Sean M. Carroll. *Spacetime and geometry: An introduction to general relativity*. 2004. ISBN: 0805387323, 9780805387322. URL: http://www.slac.stanford.edu/spires/find/books/www?cl=QC6:C37:2004.

[32] B.S. Ryden. "An Introduction to Cosmology". In: (2002).

[33] Manuel Drees, Fazlollah Hajkarim, and Ernany Rossi Schmitz. "The Effects of QCD Equation of State on the Relic Density of WIMP Dark Matter". In: *JCAP* 1506.06 (2015), p. 025. DOI: 10.1088/1475-7516/2015/06/025. arXiv: 1503.03513 [hep-ph].

[34] Gordon L. Kane et al. "Dark matter production mechanisms with a non-thermal cosmological history: A classification". In: *Phys. Rev.* D93.6 (2016), p. 063527. DOI: 10.1103/PhysRevD.93.063527. arXiv: 1502.05406 [hep-ph].

[35] Mariangela Lisanti. "Lectures on Dark Matter Physics". In: *Proceedings, Theoretical Advanced Study Institute in Elementary Particle Physics: New Frontiers in Fields and Strings (TASI 2015): Boulder, CO, USA, June 1-26, 2015*. 2017, pp. 399–446. DOI: 10.1142/9789813149441_0007. arXiv: 1603.03797 [hep-ph]. URL: https://inspirehep.net/record/1427360/files/arXiv:1603.03797.pdf.

[36] Torsten Bringmann and Stefan Hofmann. "Thermal decoupling of WIMPs from first principles". In: *JCAP* 0704 (2007). [Erratum: JCAP1603,no.03,E02(2016)], p. 016. DOI: 10.1088/1475-7516/2007/04/016,10.1088/1475-7516/2016/03/E02. arXiv: hep-ph/0612238 [hep-ph].

[37] Torsten Bringmann. "Particle models and the small-scale structure of dark matter". In: *New Journal of Physics* 11.10 (2009), p. 105027. URL: http://stacks.iop.org/1367-2630/11/i=10/a=105027.

[38] Paolo Gondolo, Junji Hisano, and Kenji Kadota. "The Effect of quark interactions on dark matter kinetic decoupling and the mass of the smallest dark halos". In: *Phys. Rev.* D86 (2012), p. 083523. DOI: 10.1103/PhysRevD.86.083523. arXiv: 1205.1914 [hep-ph].

[39] Gerard Jungman, Marc Kamionkowski, and Kim Griest. "Supersymmetric dark matter". In: *Phys. Rept.* 267 (1996), pp. 195–373. DOI: 10.1016/0370-1573(95)00058-5. arXiv: hep-ph/9506380 [hep-ph].

[40] Torsten Bringmann. "Particle Models and the Small-Scale Structure of Dark Matter". In: *New J. Phys.* 11 (2009), p. 105027. DOI: 10.1088/1367-2630/11/10/105027. arXiv: 0903.0189 [astro-ph.CO].

[41] A. Kravtsov. "The Dark Matter Annihilation Signal from Dwarf Galaxies and Subhalos". In: *Advances in Astronomy* 2010, 281913 (2010), p. 281913. DOI: 10.1155/2010/281913. arXiv: 0906.3295.

[42] A. Klypin et al. "Where Are the Missing Galactic Satellites?" In: 522 (Sept. 1999), pp. 82–92. DOI: 10.1086/307643. eprint: astro-ph/9901240.

[43] R. Kuzio de Naray and K. Spekkens. "Do Baryons Alter the Halos of Low Surface Brightness Galaxies?" In: 741, L29 (Nov. 2011), p. L29. DOI: 10.1088/2041-8205/741/2/L29. arXiv: 1109.1288.

[44] M. G. Walker and J. Peñarrubia. "A Method for Measuring (Slopes of) the Mass Profiles of Dwarf Spheroidal Galaxies". In: 742, 20 (Nov. 2011), p. 20. DOI: 10.1088/0004-637X/742/1/20. arXiv: 1108.2404.

[45] M. Boylan-Kolchin, J. S. Bullock, and M. Kaplinghat. "Too big to fail? The puzzling darkness of massive Milky Way subhaloes". In: 415 (July 2011), pp. L40–L44. DOI: 10.1111/j.1745-3933.2011.01074.x. arXiv: 1103.0007 [astro-ph.CO].

[46] M. Boylan-Kolchin, J. S. Bullock, and M. Kaplinghat. "The Milky Way's bright satellites as an apparent failure of ΛCDM". In: 422 (May 2012), pp. 1203–1218. DOI: 10.1111/j.1365-2966.2012.20695.x. arXiv: 1111.2048 [astro-ph.CO].

[47] G. Efstathiou, J. R. Bond, and S. D. M. White. "COBE background radiation anisotropies and large-scale structure in the universe". In: 258 (Sept. 1992), 1P–6P. DOI: 10.1093/mnras/258.1.1P.

[48] P. Chang, A. E. Broderick, and C. Pfrommer. "The Cosmological Impact of Luminous TeV Blazars. II. Rewriting the Thermal History of the Intergalactic Medium". In: 752, 23 (June 2012), p. 23. DOI: 10.1088/0004-637X/752/1/23. arXiv: 1106.5504.

[49] Joseph Silk and Adi Nusser. "The Massive-black-holefffdfffdfffdVelocity-dispersion Relation and the Halo Baryon Fraction: A Case for Positive Active Galactic Nucleus Feedback". In: *The Astrophysical Journal* 725.1 (2010), p. 556. URL: http://stacks.iop.org/0004-637X/725/i=1/a=556.

[50] M. A. Breddels et al. "Orbit-based dynamical models of the Sculptor dSph galaxy". In: 433 (Aug. 2013), pp. 3173–3189. DOI: 10.1093/mnras/stt956. arXiv: 1205.4712.

[51] C. A. Vera-Ciro et al. "Not too big, not too small: the dark haloes of the dwarf spheroidals in the Milky Way". In: 428 (Jan. 2013), pp. 1696–1703. DOI: 10.1093/mnras/sts148. arXiv: 1202.6061.

[52] J. Wang et al. "The missing massive satellites of the Milky Way". In: 424 (Aug. 2012), pp. 2715–2721. DOI: 10.1111/j.1365-2966.2012.21357.x. arXiv: 1203.4097.

[53] Sean Tulin, Hai-Bo Yu, and Kathryn M. Zurek. "Beyond Collisionless Dark Matter: Particle Physics Dynamics for Dark Matter Halo Structure". In: *Phys. Rev.* D87.11 (2013), p. 115007. DOI: 10.1103/PhysRevD.87.115007. arXiv: 1302.3898 [hep-ph].

[54] David N. Spergel and Paul J. Steinhardt. "Observational evidence for selfinteracting cold dark matter". In: *Phys. Rev. Lett.* 84 (2000), pp. 3760–3763. DOI: 10.1103/PhysRevLett.84.3760. arXiv: astro-ph/9909386 [astro-ph].

[55] Naoki Yoshida et al. "Collisional dark matter and the structure of dark halos". In: *Astrophys. J.* 535 (2000), p. L103. DOI: 10.1086/312707. arXiv: astro-ph/0002362 [astro-ph].

[56] Abraham Loeb and Neal Weiner. "Cores in Dwarf Galaxies from Dark Matter with a Yukawa Potential". In: *Phys. Rev. Lett.* 106 (2011), p. 171302. DOI: 10.1103/PhysRevLett.106.171302. arXiv: 1011.6374 [astro-ph.CO].

[57] Jonathan L. Feng, Manoj Kaplinghat, and Hai-Bo Yu. "Halo Shape and Relic Density Exclusions of Sommerfeld-Enhanced Dark Matter Explanations of Cosmic Ray Excesses". In: *Phys. Rev. Lett.* 104 (2010), p. 151301. DOI: 10.1103/PhysRevLett.104.151301. arXiv: 0911.0422 [hep-ph].

[58] Matthew R. Buckley and Patrick J. Fox. "Dark Matter Self-Interactions and Light Force Carriers". In: *Phys. Rev.* D81 (2010), p. 083522. DOI: 10.1103/PhysRevD.81.083522. arXiv: 0911.3898 [hep-ph].

[59] M. Vogelsberger, J. Zavala, and A. Loeb. "Subhaloes in self-interacting galactic dark matter haloes". In: 423 (July 2012), pp. 3740–3752. DOI: 10.1111/j.1365-2966.2012.21182.x. arXiv: 1201.5892.

[60] Mateusz Duch and Bohdan Grzadkowski. "Resonance enhancement of dark matter interactions: the case for early kinetic decoupling and velocity dependent resonance width". In: *JHEP* 09 (2017), p. 159. DOI: 10.1007/JHEP09(2017)159. arXiv: 1705.10777 [hep-ph].

[61] Torsten Bringmann et al. "DarkBit: A GAMBIT module for computing dark matter observables and likelihoods". In: *Eur. Phys. J.* C77.12 (2017), p. 831. DOI: 10.1140/epjc/s10052-017-5155-4. arXiv: 1705.07920 [hep-ph].

[62] K.Griest G.Juangman M.Kamionkowski. *NEUTDRIVER*. URL: https://www.ipnl.in2p3.fr/delphi/laktineh/susy/neut.html.

[63] Torsten Bringmann et al. "DarkSUSY 6 : An Advanced Tool to Compute Dark Matter Properties Numerically". In: (2018). arXiv: 1802.03399 [hep-ph].

[64] D. Barducci et al. "Collider limits on new physics within micrOMEGAs$_4$.3". In: *Comput. Phys. Commun.* 222 (2018), pp. 327–338. DOI: 10.1016/j.cpc.2017.08.028. arXiv: 1606.03834 [hep-ph].

[65] H. Baer F.E. Paige S.D. Protopopescu and X. Tata. *ISAJET 7.88*. URL: http://www.nhn.ou.edu/~isajet/.

[66] A. Arbey, F. Mahmoudi, and G. Robbins. "SuperIso Relic v4: A program for calculating dark matter and flavour physics observables in Supersymmetry". In: (2018). arXiv: 1806.11489 [hep-ph].

[67] Federico Ambrogi et al. "MadDM v.3.0: a Comprehensive Tool for Dark Matter Studies". In: (2018). arXiv: 1804.00044 [hep-ph].

[68] Mihailo Backovic, Kyoungchul Kong, and Mathew McCaskey. "MadDM v.1.0: Computation of Dark Matter Relic Abundance Using MadGraph5". In: *Physics of the Dark Universe* 5-6 (2014), pp. 18–28. DOI: 10.1016/j.dark.2014.04.001. arXiv: 1308.4955 [hep-ph].

[69] Marilyn Gordon Lawrence Shampine. "Computer Solution of Ordinary Differential Equations: The Initial Value Problem". In: (1975).

[70] Vanda Silveira and A. Zee. "Scalar Phantoms". In: *Physics Letters B* 161.1 (1985), pp. 136–140. ISSN: 0370-2693. DOI: https://doi.org/10.1016/0370-2693(85)90624-0. URL: http://www.sciencedirect.com/science/article/pii/0370269385906240.

[71] James M. Cline et al. "Update on scalar singlet dark matter". In: *Phys. Rev.* D88 (2013). [Erratum: Phys. Rev.D92,no.3,039906(2015)], p. 055025. DOI: 10.1103/PhysRevD.92.039906,10.1103/PhysRevD.88.055025. arXiv: 1306.4710 [hep-ph].

[72] Peter Athron et al. "GAMBIT: The Global and Modular Beyond-the-Standard-Model Inference Tool". In: *Eur. Phys. J.* C77.11 (2017). [Addendum: Eur. Phys. J.C78,no.2,98(2018)], p. 784. DOI: 10.1140/epjc/s10052-017-5513-2,10.1140/epjc/s10052-017-5321-8. arXiv: 1705.07908 [hep-ph].

[73] Nima Arkani-Hamed et al. "A Theory of Dark Matter". In: *Phys. Rev.* D79 (2009), p. 015014. DOI: 10.1103/PhysRevD.79.015014. arXiv: 0810.0713 [hep-ph].

[74] Junji Hisano et al. "Non-perturbative effect on dark matter annihilation and gamma ray signature from galactic center". In: *Phys. Rev.* D71 (2005), p. 063528. DOI: 10.1103/PhysRevD.71.063528. arXiv: hep-ph/0412403 [hep-ph].

[75] Torsten Bringmann et al. "Converting non-relativistic dark matter to radiation". In: (2018). arXiv: 1803.03644 [astro-ph.CO].

[76] Kfir Blum, Ryosuke Sato, and Tracy R. Slatyer. "Self-consistent Calculation of the Sommerfeld Enhancement". In: *JCAP* 1606.06 (2016), p. 021. DOI: 10.1088/1475-7516/2016/06/021. arXiv: 1603.01383 [hep-ph].

[77] Anne M. Green, Stefan Hofmann, and Dominik J. Schwarz. "The First wimpy halos". In: *JCAP* 0508 (2005), p. 003. DOI: 10.1088/1475-7516/2005/08/003. arXiv: astro-ph/0503387 [astro-ph].

[78] A. Sommerfeld. "fffdfffdber die Beugung und Bremsung der Elektronen". In: *Annalen der Physik* 403.3 (), pp. 257–330. DOI: 10.1002/andp.19314030302. eprint: https://onlinelibrary.wiley.com/doi/pdf/10.1002/andp.19314030302. URL: https://onlinelibrary.wiley.com/doi/abs/10.1002/andp.19314030302.

[79] Sam C. A. Nierop. "The Sommerfeld enhancement". PhD thesis. Groningen U., 2009. URL: http://thep.housing.rug.nl/theses/bachelor-thesis_sam-nierop.

[80] M. Hamzavi et al. "Approximate Analytical Solution of the Yukawa Potential with Arbitrary Angular Momenta". In: *Chinese Physics Letters* 29.8, 080302 (Aug. 2012), p. 080302. DOI: 10.1088/0256-307X/29/8/080302. arXiv: 1210.5886 [quant-ph].

[81] M. Lattanzi and J. Silk. "Can the WIMP annihilation boost factor be boosted by the Sommerfeld enhancement?" In: 79.8, 083523 (Apr. 2009), p. 083523. DOI: 10.1103/PhysRevD.79.083523. arXiv: 0812.0360.

[82] J. J. Sakurai and Jim Napolitano. *Modern Quantum Mechanics*. 2nd ed. Cambridge University Press, 2017. DOI: 10.1017/9781108499996.

[83] M. Cannoni. "Relativistic $< \sigma v_{\rm rel} >$ in the calculation of relics abundances: a closer look". In: *Phys. Rev.* D89.10 (2014), p. 103533. DOI: 10.1103/PhysRevD.89.103533. arXiv: 1311.4494 [astro-ph.CO].